The Thesis Committee for Srivaramangai Rajagopalan
Certifies that this is the approved version of the following thesis:

Effect of imaging conditions for reliable measurement of local strain from synthetic High Resolution Transmission Electron Microscope (HRTEM) images by Geometrical Phase Analysis (GPA)

APPROVED BY
SUPERVISING COMMITTEE:

Supervisor:

Llewellyn Rabenberg

Paulo Ferreira

Effect of imaging conditions for reliable measurement of local strain from synthetic High Resolution Transmission Electron Microscope (HRTEM) images by Geometrical Phase Analysis (GPA)

by

Srivaramangai Rajagopalan, B.Tech; M.S.E.

Thesis

Presented to the Faculty of the Graduate School of

The University of Texas at Austin

in Partial Fulfillment

of the Requirements

for the Degree of

Master of Science in Engineering

The University of Texas at Austin

December 2009

Dedication

To my husband and parents

Acknowledgements

I would like to take this opportunity to express my deep gratitude to Prof. Lew Rabenberg for his support, guidance and encouragement throughout my course of study at University of Texas at Austin. He provided a very friendly environment for me to work in. I have had several intellectually stimulating conversations with him that has trained me to think out of the box to solve any problem.

I would like to express my appreciation to Prof. Paulo Ferreira for his interest in serving as a reader for this thesis.

I gratefully acknowledge Dr. Jayhoon Chung, who helped me understand the Jems® simulation software and the GPA image processing technique. He offered me very valuable suggestions and support to complete my thesis.

I also would like to extend my thanks to Prof. Desiderio Kovar for being understanding and supportive throughout my masters program.

Finally, I am grateful to my husband, Anand Lakshmanan, and my parents for their constant encouragement, support and love.

December 2009

Abstract

Effect of imaging conditions for reliable measurement of local strain from synthetic High Resolution Transmission Electron Microscope (HRTEM) images by Geometrical Phase Analysis (GPA)

by

Srivaramangai Rajagopalan, MSE

The University of Texas at Austin, 2009

SUPERVISOR: Llewellyn Rabenberg

Synthetic HRTEM images are simulated using Jems® simulation software with a model specimen consisting of a film of strained silicon on top of a relaxed $Si_{0.82}Ge_{0.18}$ alloy substrate in the [110] zone axis, where biaxial tensile strain exists in the strained silicon layer. Two simulated models are created: one with a sudden change in lattice constant (strained Si on a "fat" Si substrate) and another with a sudden change in atomic number (strained Si on a Cl substrate) in order to separate the effects of strain discontinuities from atomic number discontinuities measuring strain using Geometric Phase Analysis (GPA). The simulated models are subjected to image processing using GPA software developed by Chung. Two dimensional strain maps are reconstructed and the local strain is determined. Further, an analysis is done to evaluate the best imaging conditions for strain measurement using GPA at heteroepitaxial interfaces.

In addition, the behavior of GPA across a step function in strain or atomic number is examined for information about (a) spatial resolution, (b) the effects of a sudden

change in atomic number, (c) instrument parameters, and (d) specimen thickness for a 300KeV TEM.

Table of Contents

List of Tables

List of Figures

CHAPTER 1: INTRODUCTION

The continuous and systematic increase in transistor density, guided by CMOS scaling theory [1] and described in "Moore's Law" [2], has been highly successful for the development of silicon technology. Technological improvisation has indeed led to significant miniaturization of electron devices such that the number of transistors that can be placed inexpensively on an integrated circuit has doubled approximately every two years. Miniaturization has, in turn, led to increases in performance and reduction in size of electronic equipment.

With CMOS devices well below 50nm technology node, new materials and processes have been infused into the device fabrication processes in order to improve device characteristics for enhanced performance. Increase in performance of transistors can be achieved by decreasing the device scale or by increasing the carrier mobility of Si-CMOS devices. For example, aluminum metal lines used for interconnects were replaced by copper metal lines to support the shrinkage in device scale. Replacing existing materials is one option, but modifying the properties of existing materials is another possible option. Along those lines, strained silicon is a promising option for enhanced carrier mobility [3, 4]. When compressive strain is introduced into silicon, the electronic band structure is modified such that scattering of carriers within the bands is reduced and mobility of carriers is improved. Because it is possible to create large strains in device structures, it is necessary to have a technique to quantify two-dimensional strain near the device channel at the nanoscale level.

Many techniques such as x-ray diffraction (XRD) [5] Raman spectroscopy [6] and photoreflectance [7] are available to characterize strain at the wafer level. In order to resolve local strains near active devices, transmission electron microscopy (TEM)

techniques can be used. Of these, convergent beam electron diffraction (CBED) [8, 9, 10, 11] and nano-beam diffraction (NBD) [12] in TEM have been demonstrated for local strain measurement although it is very difficult to obtain two-dimensional strain images from these methods.

A promising approach to strain measurement is to use high-resolution transmission electron microscope (HRTEM) images to measure local strains in two-dimensions. HRTEM images record positions of atomic planes in a crystal that can be used to quantify strain by applying Geometric Phase Analysis (GPA) technique .GPA is a technique that uses numerical processing of HRTEM images to produce quantitative maps of displacement or strain at the nanoscale [13, 14, 15]. According to Hytch, this method can detect the atomic plane displacement to an accuracy of 0.003nm [16]. In this section, formation of a HRTEM image is discussed to understand the theory behind the evolution of GPA technique.

1.1 HIGH-RESOLUTION IMAGE FORMATION IN TEM

HRTEM images are phase contrast images, and it is well known that atomic planes may image bright or dark depending on specimen thickness or instrumental parameters. Hence, contrast shifts cannot be simply associated with displacements of atomic planes. In the traditional view, it would be necessary to know the phases of all the electron waves as they propagate down the column in order to extract information about atomic displacements. Under favorable conditions, GPA can extract strain information from HRTEM images, but it is still necessary to be familiar with the HRTEM image formation process.

Figure 1.1 shows a typical TEM column [17]. The specimen is irradiated by a nearly parallel beam of electrons. The beam transmitted through the specimen is focused to a crossover by the objective lens positioned below the specimen. An inverted, magnified, image of the specimen appears at the image plane of the objective lens.

To obtain an HRTEM image, an objective aperture that is large enough to include beams out to the information limit of the objective lens is placed around the forward beam and simultaneously around the optic axis of the objective lens. Intermediate apertures positioned below the objective aperture (not shown in Figure 1.1) are removed. A medium or small condenser aperture must be in the column and centered.

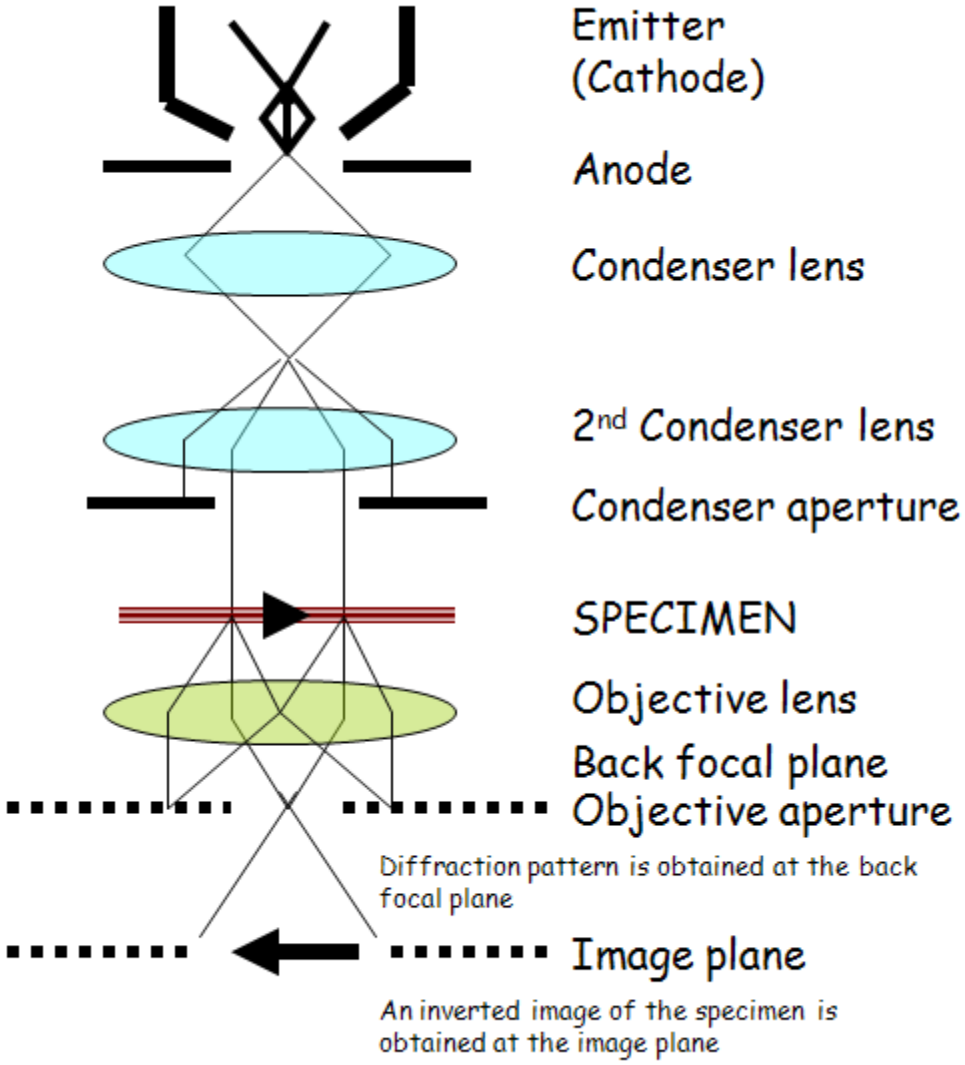

Figure 1.1: TEM column.

Figure 1.2 shows the development of phase information in the electron beam of the TEM. As a parallel electron beam transmits through a thin crystalline specimen, the areas of the wave that pass near the atomic nuclei are phase-advanced relative to those

that pass between the atomic columns. The phase modulation of the exit wave carries specimen information into the final image.

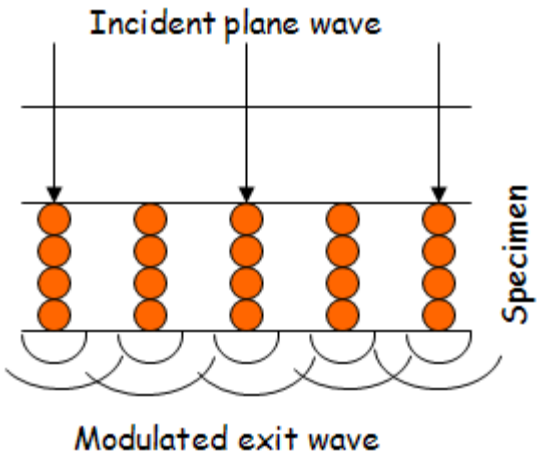

Figure 1.2: Development of phase information in the TEM.

1.2 STRAINED SILICON

A specimen suitable for the study of strained silicon on $Si_{1-x}Ge_x$ can be fabricated as shown in Figure 1.3 (a) [18]. As seen in the figure, active strained silicon is grown epitaxially on the relaxed $Si_{1-x}Ge_x$ layer. Strain is induced in the top silicon layer as a result of lattice constant mismatch between the two layers. Figure 1.3 (b) shows a typical structure of fabricated strained silicon. A layer of polycrystalline silicon is deposited over the strained layer prior to TEM specimen preparation in order to minimize atomic plane displacements during specimen thinning.

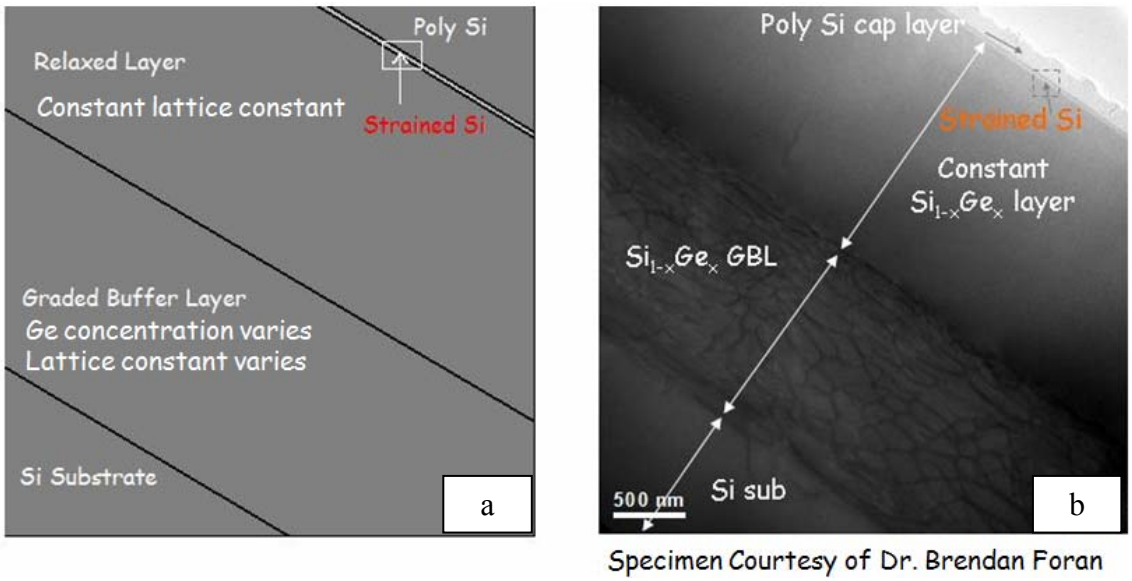

Figure 1.3: (a) Schematic diagram of a strained silicon test structure and (b) Cross sectional TEM image of a strained silicon wafer

The lattice constant of relaxed $Si_{1-x}Ge_x$ alloy, 0.5525nm, is greater than that of silicon, 0.5431nm. Coherency stresses result in a tetragonal distortion of the silicon epitaxial layer as shown in Figure 1.4.

The lattice constant of the heterostructure formed from two cubic structures of lattice constants, a_m and a_n are given as follows, under the constraint that the lattice constant parallel to the plane of the hetero-interface remains the same throughout the structure [19]:

$$a_{||} = \frac{a_n G_n h_n + a_m G_m h_m}{G_n h_n + G_m h_m}, \tag{1.1a}$$

$$a_{i\perp} = a_i (1 - \frac{2C_{12}^i}{C_{11}^i}(\frac{a_{||}}{a_i} - 1)), \tag{1.1b}$$

where i indicates materials m or n, $a_{||}$ is the lattice constant of the heterostructure parallel to the plane of the hetero-interface, $a_{\perp}$ is the lattice constant of heterostructure perpendicular to the interface plane, a_i are the lattice constants of m or n, when they form bulk materials, and h_i are the thicknesses of the materials. If it is assumed that h_m is infinite, $a_{||} = a_m$. G_i^{001} is the shear modulus in the <100> directions within the (001) plane given by [19]:

$$G_i^{001} = 2(C^i_{11} + 2C^i_{12})(1 - \frac{C^i_{12}}{C^i_{11}}), \tag{1.2}$$

Where, C_{11} and C_{12} are elastic constants. The elastic constants and lattice constants of Si, Ge, and $Si_{1-x}Ge_x$ alloys are summarized in Table 1.1, where the values for $Si_{1-x}Ge_x$ alloys have been linearly interpolated.

Lattice constant mismatches between a strained epitaxial layer and the reference lattice results in a cumulative displacement, u_n, as shown schematically in Figure 1.4. Under favorable conditions, an HRTEM image of the heterostructure shows positions of the atomic planes in both materials so that it is possible to determine the displacement that is defined as the difference between real atomic position and reference lattice position as follows [20]:

$$u_n = \sum_{1}^{n} (a_{n\perp} - a_m), \tag{1.3}$$

where $a_{n\perp}$ and a_m are defined as in Figure 1.4.

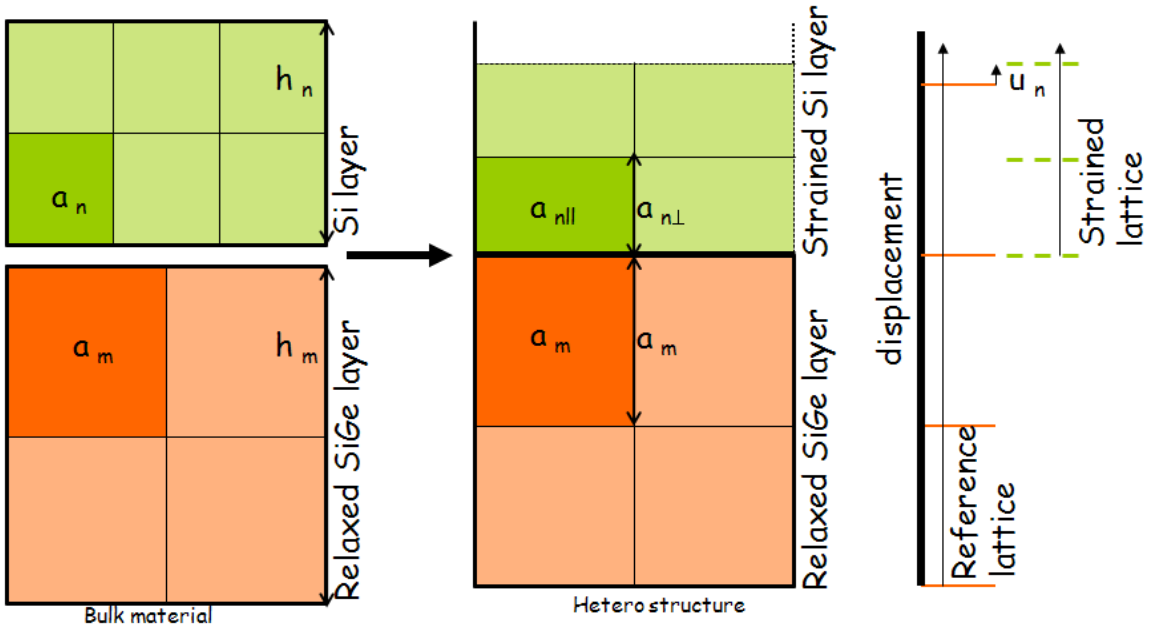

Figure 1.4: Schematic of heterostructure formed from two bulk materials with different lattice constants.

Properties	**Si**	**Ge**	**$Si_{1-x}Ge_x$**
Lattice Constant (nm)	0.5431	0.5646	(1-x) a_{Si} + x a_{Ge}
C11 (GPa)	165.7	128.5	(1-x) C^{Si}_{11} + x C^{Ge}_{11}
C12 (GPa)	63.9	48.3	(1-x) C^{Si}_{12} + x C^{Ge}_{12}

Table 1.1: Physical data for Si, Ge and Si1-xGex alloy.

1.3 GEOMETRIC PHASE ANALYSIS

The HRTEM image displays mainly phase contrast that is due to the phase differences between electrons in the forward beam and electrons in each diffracted beam. The details of the contrast in the phase image depend on the specimen, specimen orientation and instrumental parameters. The conversion from phase information to intensity information is not simple and intuitive as the phase differences are converted to intensity differences through the action of the imperfect objective lenses. Thus computer simulations and image processing are needed to know the atomic positions at an interface at accuracy better than the point resolution of the TEM.

As discussed earlier, an HRTEM image is a periodic array of dots imaging bright or dark depending on the experimental parameters. They should be exactly periodic within areas where specimen thickness, average atomic number, and specimen orientation are constant. Any deviations from this periodicity will be readily detected through Fourier analysis; this is the basis for GPA.

In GPA, the HRTEM image is Fourier-transformed, yielding a power spectrum with the same geometry as a selected-area diffraction pattern from the same area of the specimen. Two peaks in the power spectrum are selected. Each is individually moved to the center of Fourier space, masked, and inverse-transformed. By moving the peak to the center before inverse transformation, the periodic part of the image is eliminated, leaving only the deviations from perfect periodicity. If this is done for each of two non-collinear reflections, it is possible to resolve the resulting strains in any direction within the plane of the specimen. Hence, strain information can be obtained by Fourier analysis of the deviations from periodicity in a HRTEM image without necessarily knowing all the instrument and specimen parameters.

1.4 SCOPE OF THIS STUDY

The primary objectives of this study are to examine the behavior of GPA across a step function in strain in order to derive information about (a) spatial resolution, (b) the effects of a sudden change in atomic number, (c) instrument parameters, and (d) specimen thickness. HRTEM images from a model specimen having a step function in strain or atomic number will be simulated using Jems® simulation software. These synthetic HRTEM images will be subjected to GPA image processing using software developed by Chung. In this study, synthetic HRTEM images will be simulated [21] with a model of strained silicon on top of a relaxed $Si_{1-x}Ge_x$ alloy substrate in [110] zone axis, where biaxial tensile strain exists in the strained silicon layer. The following sections describe the set of experiments that will be performed using GPA technique in this study.

A secondary objective of this study is to evaluate best imaging conditions for GPA. Chung and Rabenberg have proposed that GPA is best conducted on images taken such that $\nabla_k \chi(\mathbf{k}) = 0$ (where $\nabla_k \chi(\mathbf{k})$ is the gradient of the phase contrast transfer function), but their analysis neglected sudden changes in atomic number that occur at heteroepitaxial interfaces. In addition, their analysis neglected dynamical effects. It is of interest to know how these approximations affect strain measurements.

1.4.1. Effect of a Sudden Change in Average Atomic Number

The critical parameters in creating a Jems® crystal file to simulate HRTEM images are the local interatomic spacings and the form factors of the elements present in the crystal. Although the form factors are automatically generated into the Jems® file at the time the crystal file is loaded into the simulation software, the interatomic spacings must be clearly defined by the user.

In this study, alternative to Chung's model, each atomic site represented by $Si_{1-x}Ge_x$ alloy substrate is represented by an average atom. In this case, an average atom number would be [4X14 (Si) + 1X32 (Ge)]/5 = 17.6, which is between chlorine and argon. So, a $S_{1-x}G_x$ alloy with 18% Ge is represented by an average atom, chlorine. Hence, chlorine form factors with $Si_{82}Ge_{18}$ lattice constants (assuming a linear Vegard's law for atomic form factors) are used to represent the model of strained silicon on top of a relaxed $Si_{82}Ge_{18}$ alloy substrate to study the effects of sudden change in atomic number on measurement of strain.

The following imaging conditions are used to create HRTEM images using the Jems® software. A multislice calculation with separate slices for each atomic layer is performed in order to create the HRTEM image.

Electron beam energy: 300KeV (λ = 0.00196 nm)

Spherical aberration coefficient of the objective lens, C_s: 1.2 mm

Chromatic aberration coefficient, C_c: 1.1 mm

Convergence half-angle: 1.0 mrad

Defocus spread: 4.5 nm

2-fold and 3-fold astigmatism and axial coma are ignored in this simulation

In this case, there is a sudden change in atomic number with no attendant change in d-spacings.

1.4.1.1. Effect of Defocus on Measurement of Strain

HRTEM images of strained silicon on top of $Si_{82}Ge_{18}$ alloy substrate will be simulated using Jems® simulation software for a sample thickness of ~10nm with various defocus values ranging from -57nm to -38nm. The simulated images will be processed using the

GPA technique using the {111} Bragg beams from which the local strain will be quantified. The strain calculated from the GPA technique will be compared with the actual strain from the following equation to determine the optimum defocus [18].

$$e_{n\perp} = \left(\frac{a_{n\perp} - a_m}{a_m}\right) \tag{1.4}$$

1.4.1.2. Effect of Sample Thickness on Measurement of Strain

HRTEM images will be simulated using Jems® simulation software for the optimum defocus for sample thicknesses 10 nm, 20 nm, 30 nm, 40 nm and 50 nm for a model of strained silicon on top of a $Si_{82}Ge_{18}$ alloy substrate in the [110] zone axis. The GPA technique will be used to quantify the local strain induced in silicon by analyzing the {111} Bragg beams. The strain calculated from the GPA technique will be compared to the actual strain calculated from Equation (1.4) to determine the optimum thickness for performing GPA.

1.4.1.3. Effect of C_s-Corrected Microscope on Measurement of Strain

HRTEM images will be simulated using Jems® simulation software for the optimum defocus and sample thickness for a slightly negative coefficient of spherical aberration (-5 μm) in order to emulate a Cs-corrected microscope. The calculated strain from the GPA technique will be compared and analyzed with the actual strain from Equation (1.4).

1.4.2. Comparison with "Fat" Silicon

A Jems® crystal file will be created with Si atoms replacing all the atomic sites of $Si_{1-x}Ge_x$ alloy substrate. The interatomic spacings are maintained as before but the form factors of silicon will be included in the crystal file instead of that of Cl. The strain calculated from GPA technique will be compared and analyzed with results from section 1.4.1. In this case, there is a sudden change in lattice constant with no change in atomic number.

CHAPTER 2: SIMULATION RESULTS

2.1 EFFECT OF A SUDDEN CHANGE IN AVERAGE ATOMIC NUMBER

Synthetic HRTEM images with known strain of 1.26% were created using Jems® software. As mentioned in the introduction, the $Si_{0.82}Ge_{0.18}$ alloy is represented by form factors for an average atom, Cl. The model for the simulated HRTEM images consists of a layer of strained Si on a relaxed, semi-infinite Cl substrate as shown in Figure 2.1, where biaxial tensile strain exists only in the strained Si layer. The Ge concentration of the relaxed area controls the strain in the strained Si layer. The relative strain was calculated by the mismatch perpendicular to the hetero-interface using Equation (1.4). The atomic positions of the sSi (strained Si) layer in Figure 2.1 are displaced in the [001] direction according to Equation (1.3).

The HRTEM images were simulated using the following imaging conditions is shown in Figure 2.2.

Electron beam energy: 300KeV (λ = 0.00196 nm)

Spherical aberration coefficient of the objective lens, *Cs*: 1.2 mm

Chromatic aberration coefficient, C_c: 1.1 mm

Convergence half-angle: 1.0 mrad

Defocus change: -47 nm

Thickness of sample: ~10nm

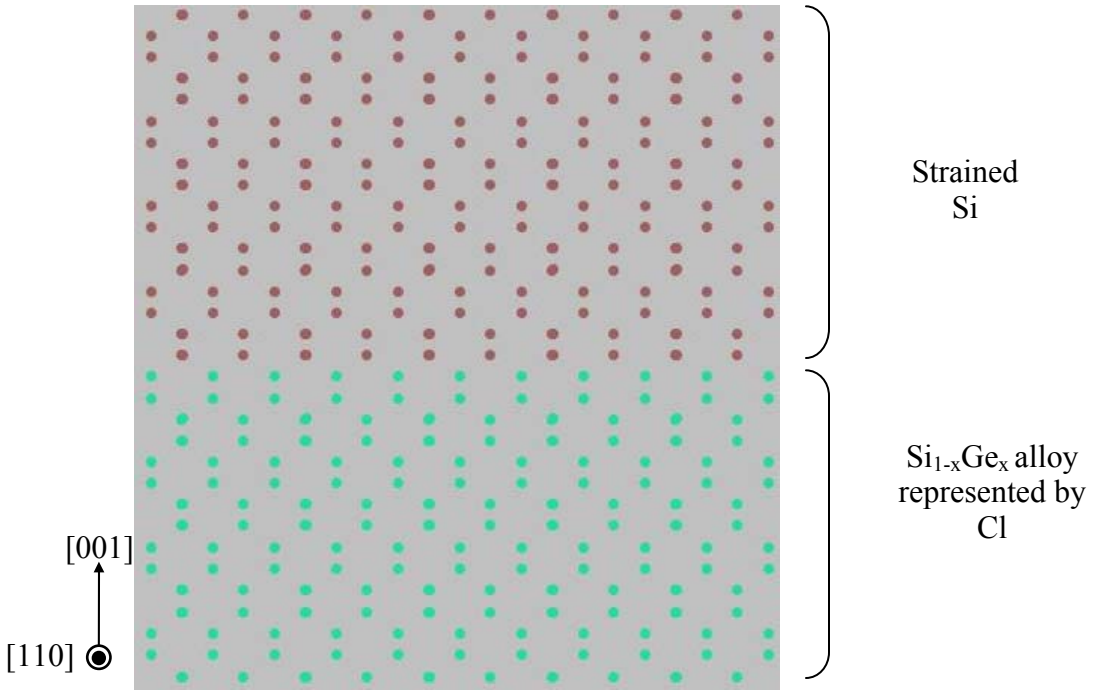

Figure 2.1: Atomic arrangement of sSi layer on relaxed $Si_{0.82}Ge_{0.18}$ alloy by Jems.

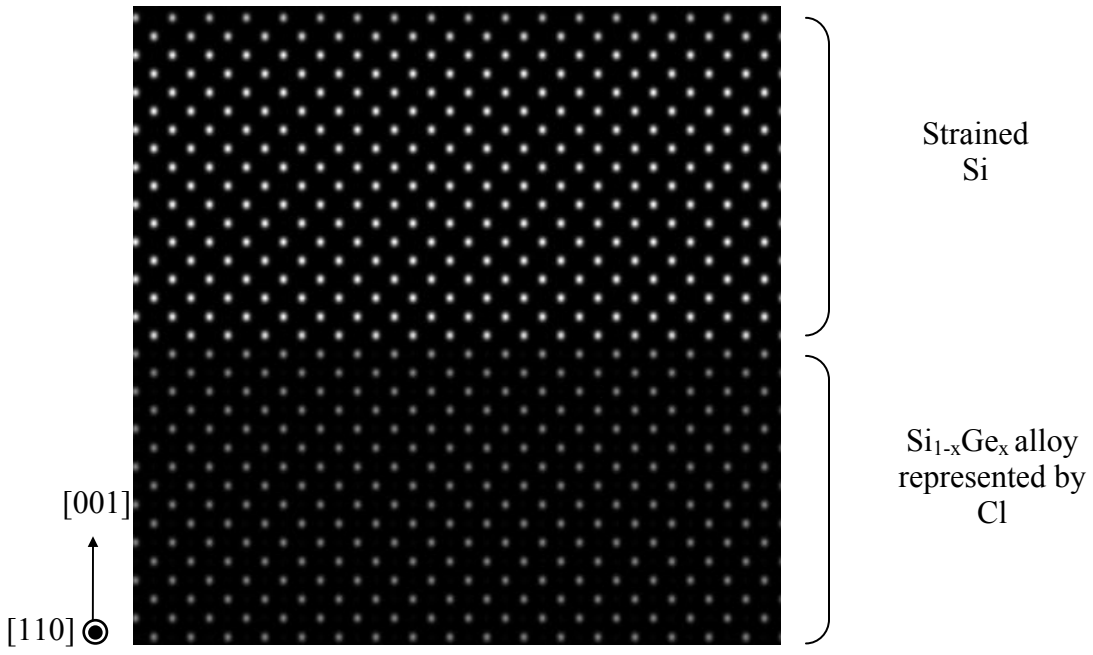

Figure 2.2: Simulated HRTEM image of sSi layer on relaxed $Si_{0.82}Ge_{0.18}$ by Jems.

It can be noted that the dumbbells expected for HRTEM image when viewing diamond structure in <110> direction are not resolved for the particular imaging conditions simulated here. This will also be true for most of the simulated images throughout the remainder of this chapter.

2.1.1. Effect of Defocus on Apparent Strains Measured using {111} Beams

The purposes of this section are to examine the variation of measured strains with respect to changes in defocus and to determine the optimum defocus for accurate strain determination using the GPA technique from {111} Bragg beam from Si specimens.

As mentioned in introduction chapter, the best imaging conditions as described by Chung and Rabenberg requires that $\nabla_k \chi(\mathbf{k})$, the gradient of the phase contrast transfer function, to be zero where that $\nabla_k \chi(\mathbf{k})$ is given by,

$$\nabla_k \chi(\mathbf{k}) = 2\pi C_S \lambda^3 \mathbf{k}^3 + 2\pi \Delta f \lambda \mathbf{k} . \qquad (2.1)$$

Using $\mathbf{k}$ = 3.18 nm^{-1} for {111} beams in Si, C_s = 1.2 mm, and λ = 0.00196 nm, the Δf meeting the condition that $\nabla_k \chi(\mathbf{k})$ is zero is found to be -47 nm from Equation (2.1).

HRTEM images of a sSi layer on relaxed $Si_{82}Ge_{18}$ with $e_{n\perp}$ = -1.26 %, were simulated for various defocus values, keeping all other imaging conditions (C_s, C_c, λ, convergence half angle and sample thickness) constant. Figure 2.3 (a) through Figure 2.9 (a) show HRTEM images for Δf = -38 nm, Δf = -41nm, Δf = -44nm, Δf = -47nm, Δf = -50nm, Δf = -53nm and Δf = -56 nm, respectively. Each of these simulated images was processed using GPA and reconstructed as a strain map following the sequences developed by Chung. Figure 2.3 (b) through Figure 2.9 (b) show the reconstructed strain

images for the same defocus values. Line-scan plots are displayed for each strain map in Figure 2.3 (c) through Figure 2.9 (c).

Table 2.1 shows the mismatch values measured from the line scan plots for each HRTEM image. The average strain values and their standard deviation were measured in the center region of each strained layer in each line plot as shown in Figure2.3 (c) in order to exclude the effect of artifacts near interface. These results indicated that the measured mismatch values were in very close agreement (within 0.03% variation) with the preset values for cases when Δf varied from -38nm to -47nm (optimum defocus). At the optimum defocus, a change in trend is noticed in the measured strain values as shown in Figure 2.10. The measured mismatch values changed by ~ 0.08% for a change in Δf of -3nm for cases when Δf is greater than the optimum defocus and also significant oscillations were noticed near the interface. The strain mismatch value measured at the optimum defocus was -1.23% ± 0.018%.

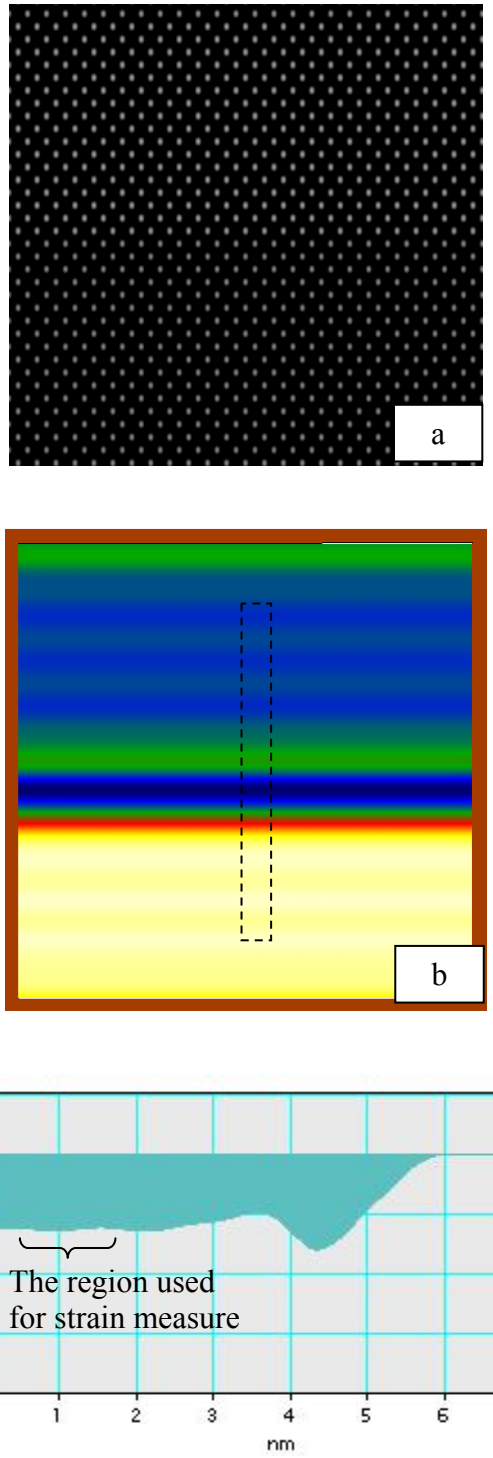

Figure 2.3: (a) HRTEM image of sSi on Cl substrate for Δf = -38nm, (b) relative strain map of (a), and (c) line-scan plot of the dotted area in (b).

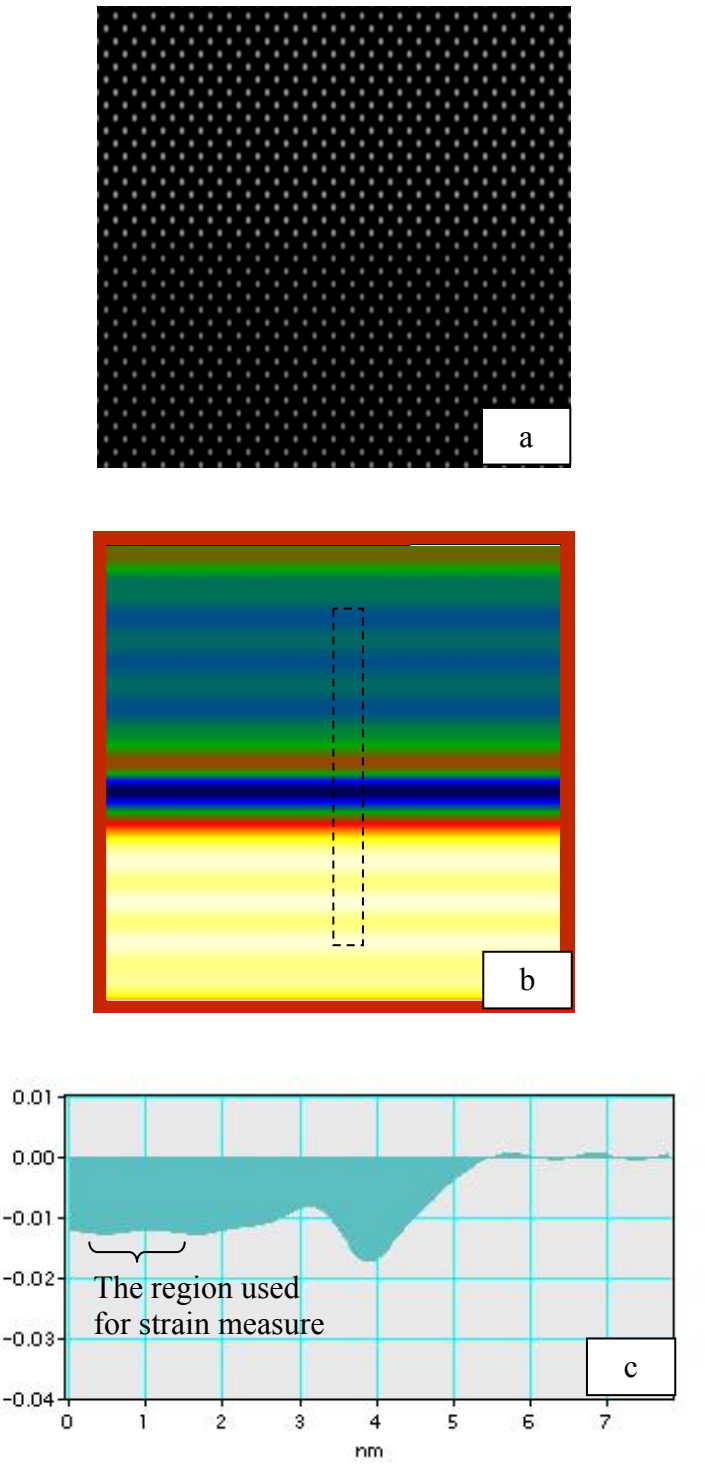

Figure 2.4: (a) HRTEM image of sSi on Cl substrate for Δf = -41nm, (b) relative strain map of (a), and line-scan plot of the dotted area in (b).

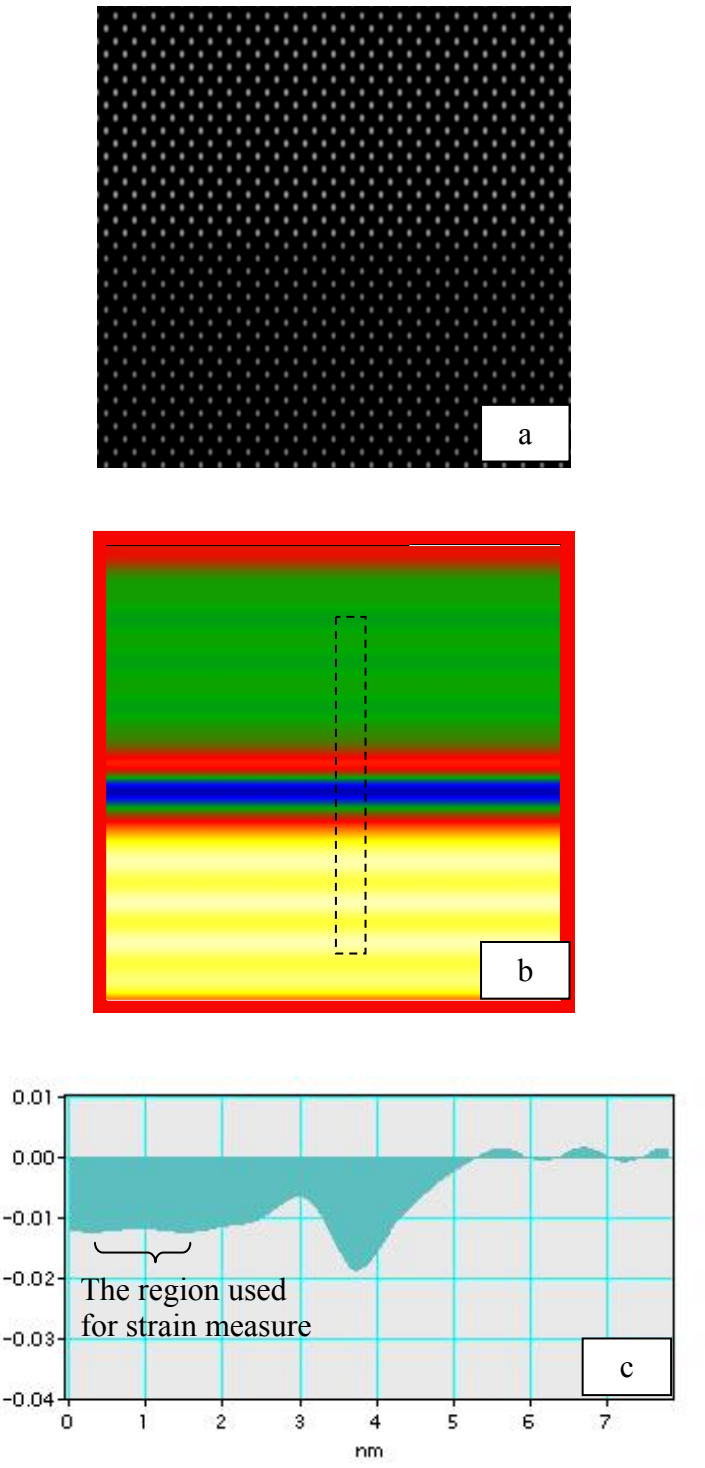

Figure 2.5: (a) HRTEM image of sSi on Cl substrate for Δf = -44nm, (b) relative strain map of (a), and line-scan plot of the dotted area in (b).

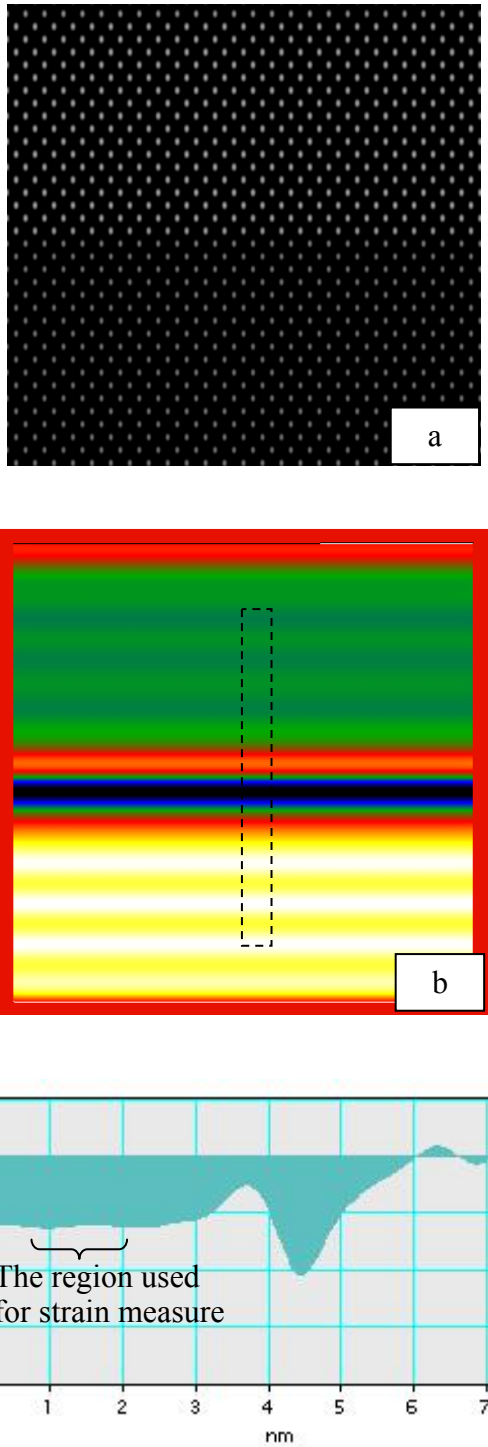

Figure 2.6: (a) HRTEM image of sSi on Cl substrate for Δf = -47nm, (b) relative strain map of (a), and line-scan plot of the dotted area in (b).

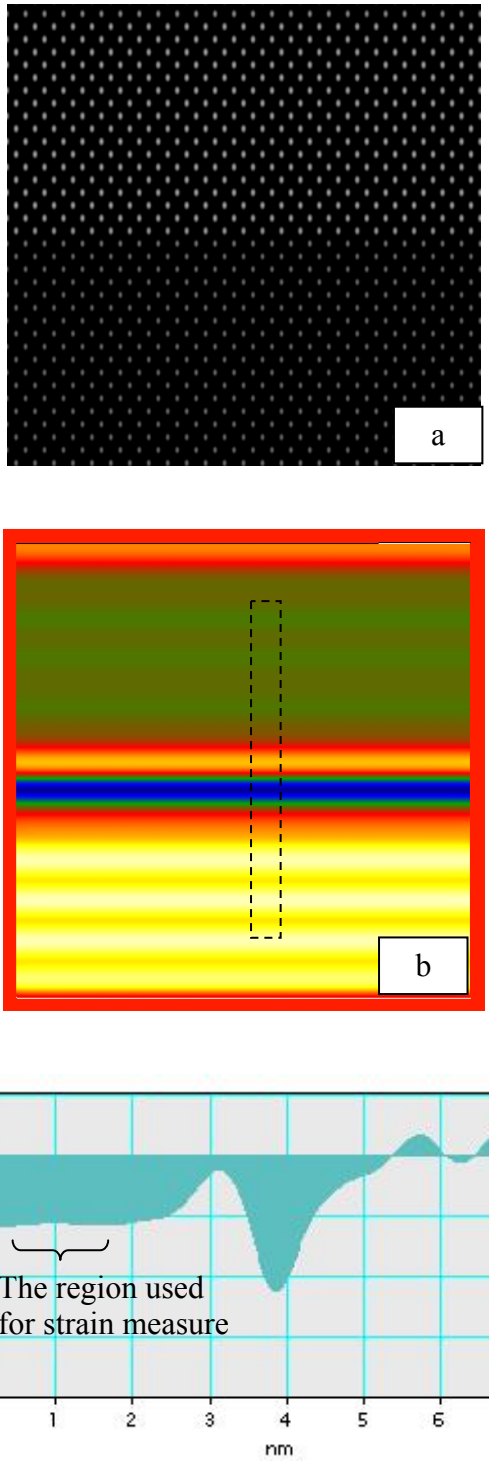

Figure 2.7: (a) HRTEM image of sSi on Cl substrate for Δf = -50nm, (b) relative strain map of (a), and line-scan plot of the dotted area in (b).

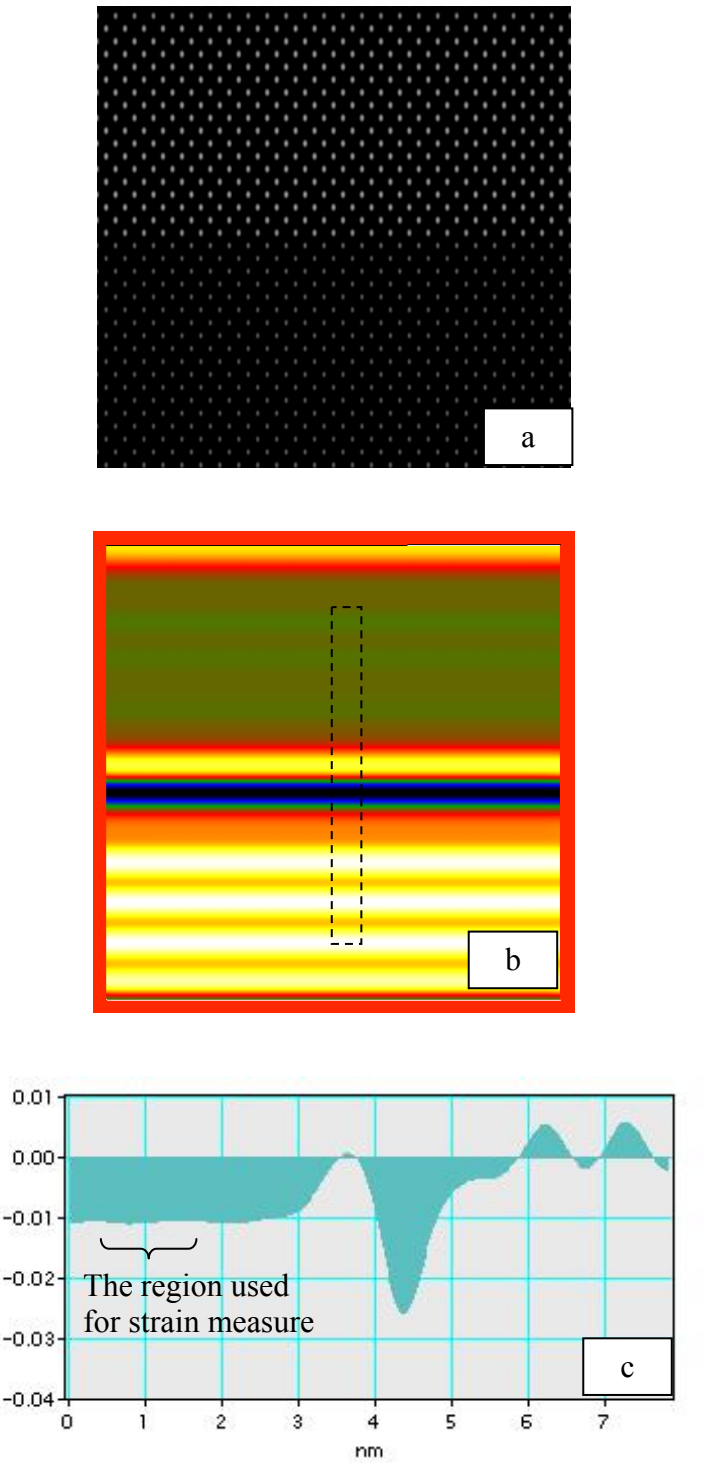

Figure 2.8: (a) HRTEM image of sSi on Cl substrate for Δf = -53nm, (b) relative strain map of (a), and line-scan plot of the dotted area in (b).

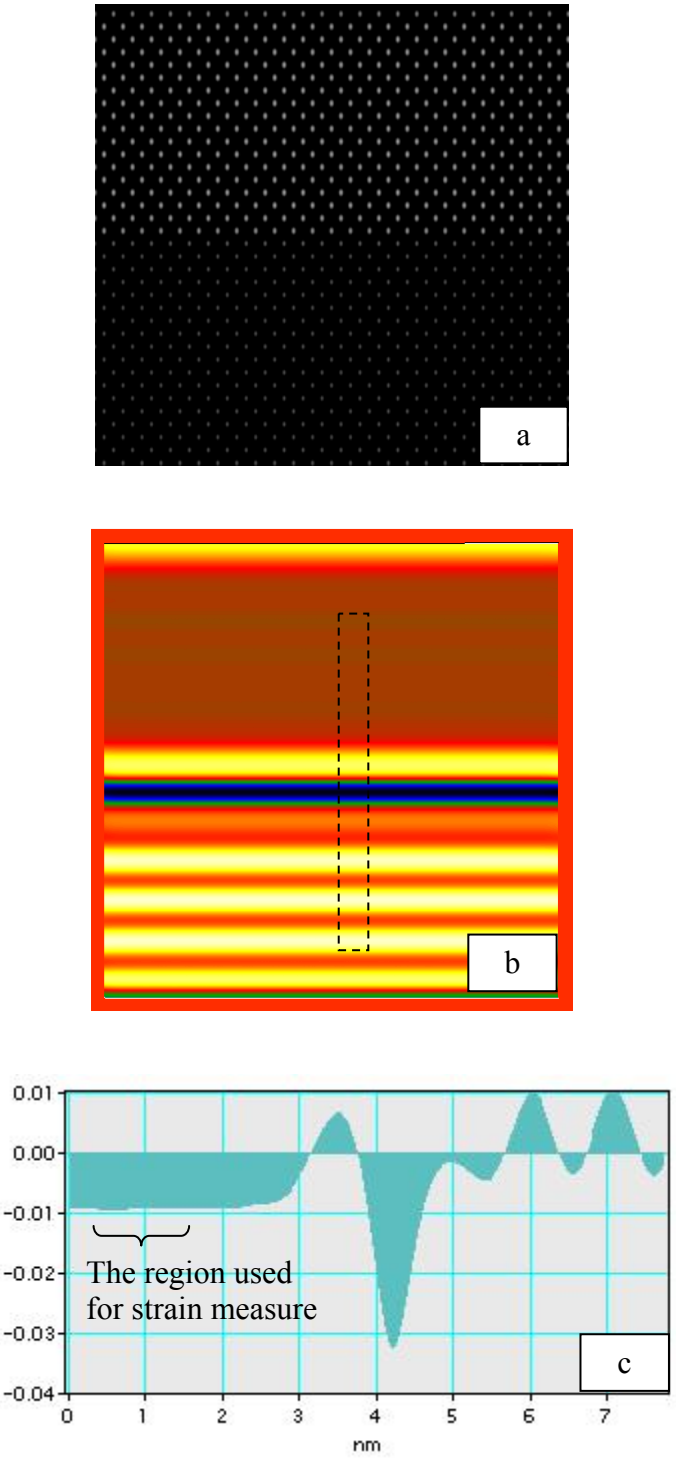

Figure 2.9: (a) HRTEM image of sSi on Cl substrate for Δf = -56nm, (b) relative strain map of (a), and line-scan plot of the dotted area in (b).

Relaxed area, $Si_{0.82}Ge_{0.18}$ Δf (nm)	**Mismatch (Relative strain, $e_{n\perp}$)**		
	Preset (%)	**Measured**	
		Average (%)	**Standard deviation (%)**
-38	-1.26	-1.2600	0.0222
-41	-1.26	-1.2410	0.0210
-44	-1.26	-1.2153	0.0203
-47	-1.26	-1.2304	0.0176
-50	-1.26	-1.1486	0.0165
-53	-1.26	-1.0741	0.0160
-56	-1.26	-0.9238	0.0170

Table 2.1: Preset and measured mismatch data for sSi on Cl substrate for different Δf values.

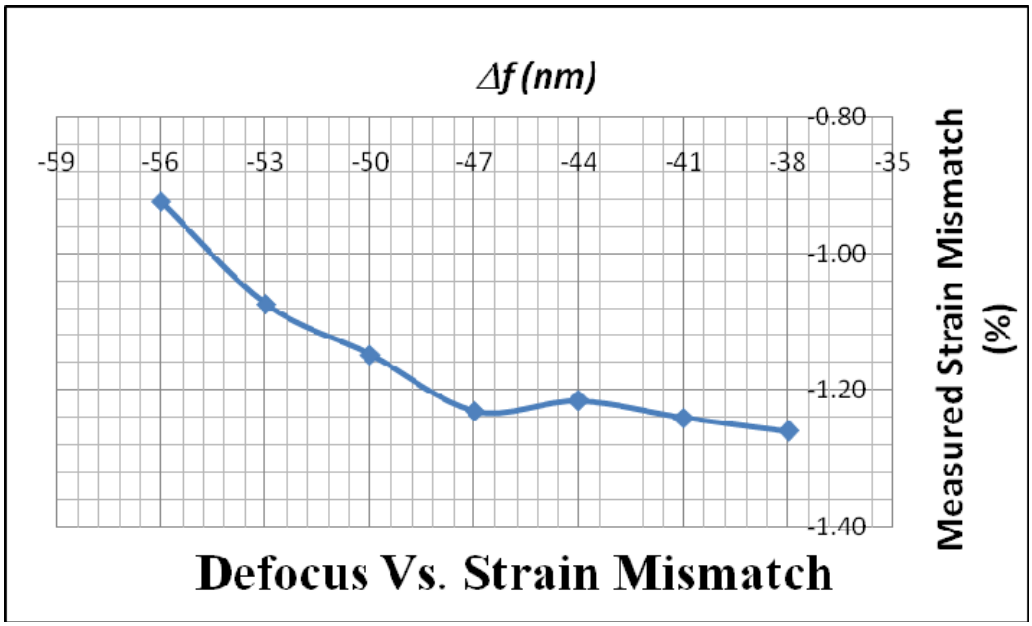

Figure 2.10: Preset and measured mismatch data for sSi on Cl substrate for different Δf values.

2.1.2 Effect of Sample Thickness on Measurement of Strain

The purpose of this section is to understand the variation of strain with respect to change in sample thickness and to determine the optimum thickness to characterize strain using GPA technique from {111} Bragg beams.

HRTEM images of sSi layer on relaxed $Si_{82}Ge_{18}$ with $e_{n\perp}$ = -1.26 %, were simulated for sample thickness 10 nm, 20 nm, 30 nm, 40 nm and 50 nm with the following conditions:

Electron beam energy: 300KeV (λ = 0.00196 nm)

Spherical aberration coefficient of the objective lens, *Cs*: 1.2 mm

Chromatic aberration coefficient, C_c: 1.1 mm

Convergence half-angle: 1.0 mrad

Defocus change: -47 nm

$Si_{72}Ge_{18}$ with $e_{n\perp}$ = -1.26 %

Figure 2.11 (a) through Figure 2.15 (a) show HRTEM images for sample thicknesses of 10 nm, 20 nm, 30 nm, 40 nm and 50 nm, respectively. Figure 2.11 (b) through Figure 2.15 (b) show the reconstructed strain images for the same thickness values. Line-scan plots are displayed for each strain map in Figure 2.11 (c) through Figure 2.15 (c).

Table 2.2 shows the mismatch values measured from the line scan plots for each HRTEM image. The average strain values and their standard deviation were measured in the center region of each strained layer in each line plot as shown in Figure 2.11 (c) in order to exclude the effect of artifacts near interface.

As expected, with the increase in sample thickness, significant oscillations were observed near the interface. For a sample of 30 nm thickness, the HRTEM image showed a shift in the atomic plane at the interface. With further increase in sample thickness, the contrast in the HRTEM image was reversed. Table 2.2 shows the mismatch values measured from the line scan plots for each HRTEM image. These results indicated that the measured mismatch values were in close agreement with the preset values for sample of thickness 10 nm and 20 nm. The measured mismatch values varied significantly from preset value for cases with sample thickness varying from 30 nm through 50 nm.

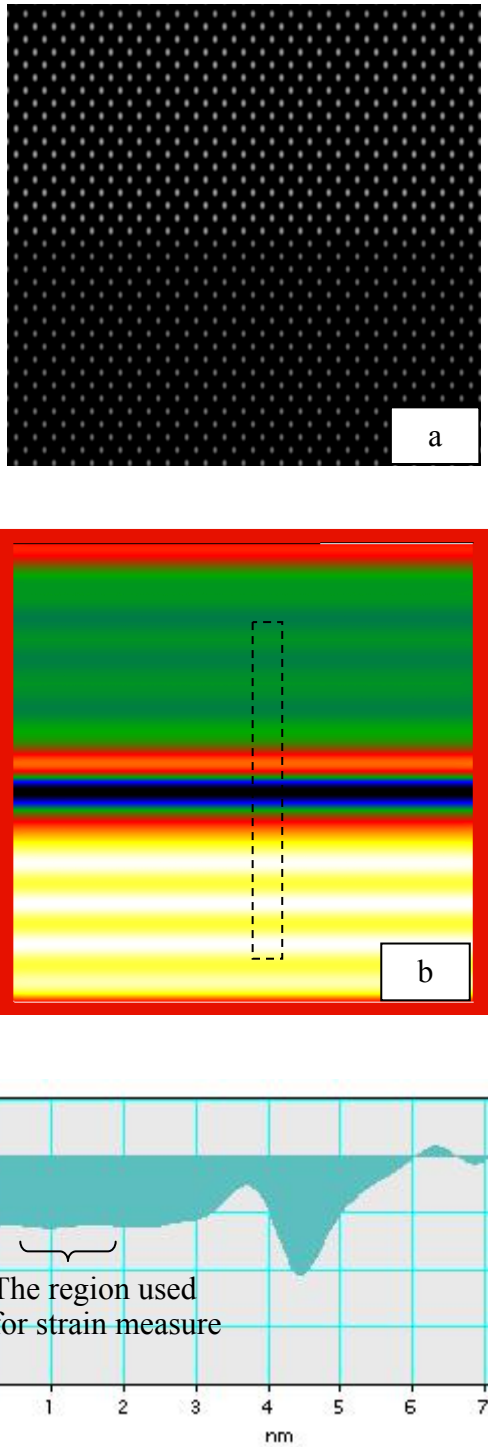

Figure 2.11: (a) HRTEM image of sSi on Cl substrate for *thickness* = 10nm, (b) relative strain map of (a), and line-scan plot of the dotted area in (b).

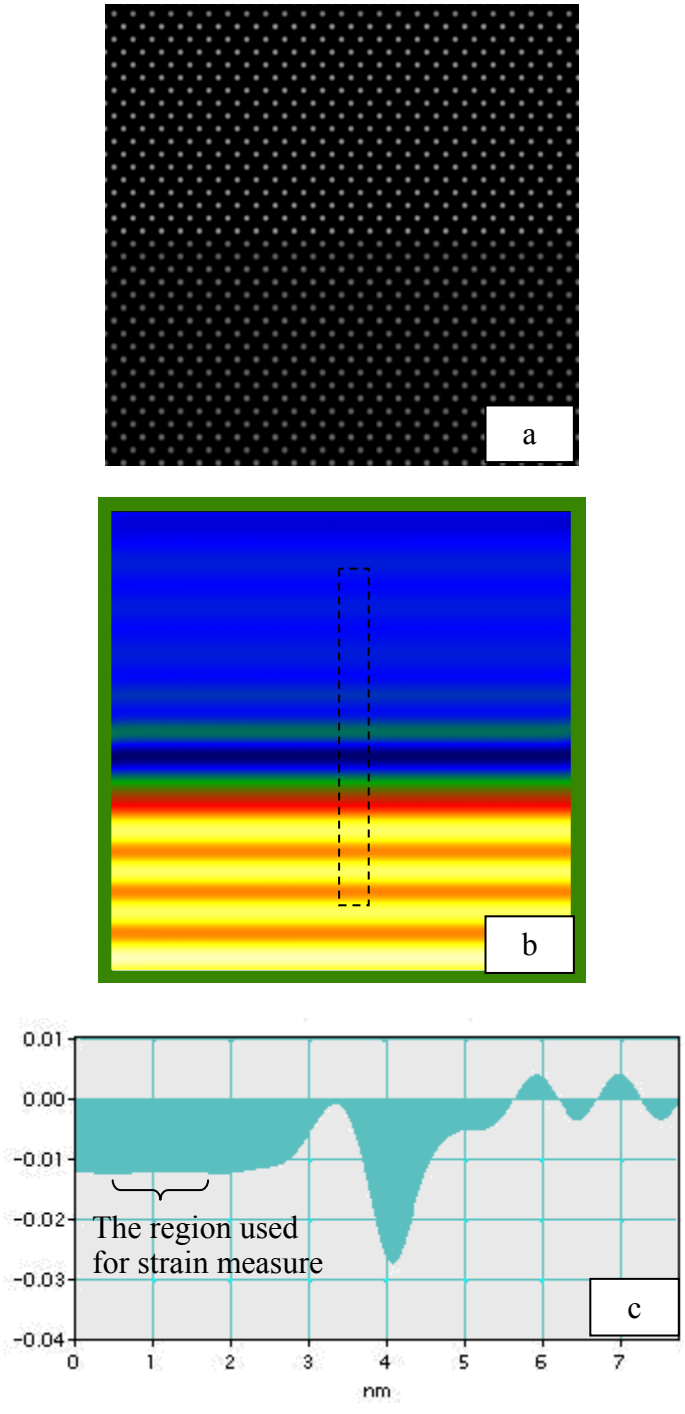

Figure 2.12: (a) HRTEM image of sSi on Cl substrate for *thickness* = 20nm, (b) relative strain map of (a), and line-scan plot of the dotted area in (b).

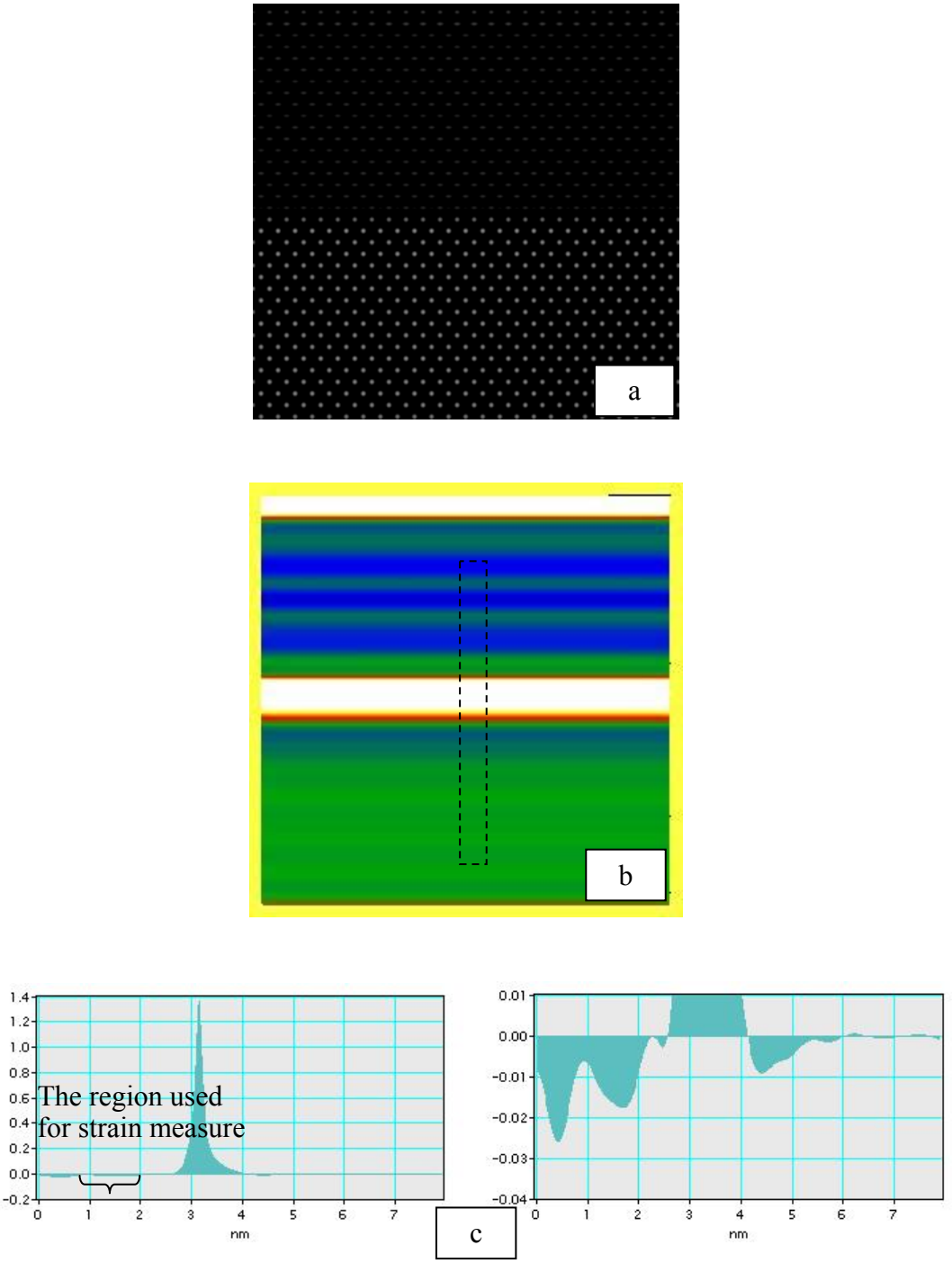

Figure 2.13: (a) HRTEM image of sSi on Cl substrate for *thickness* = 30nm, (b) relative strain map of (a), and line-scan plot of the dotted area in (b).

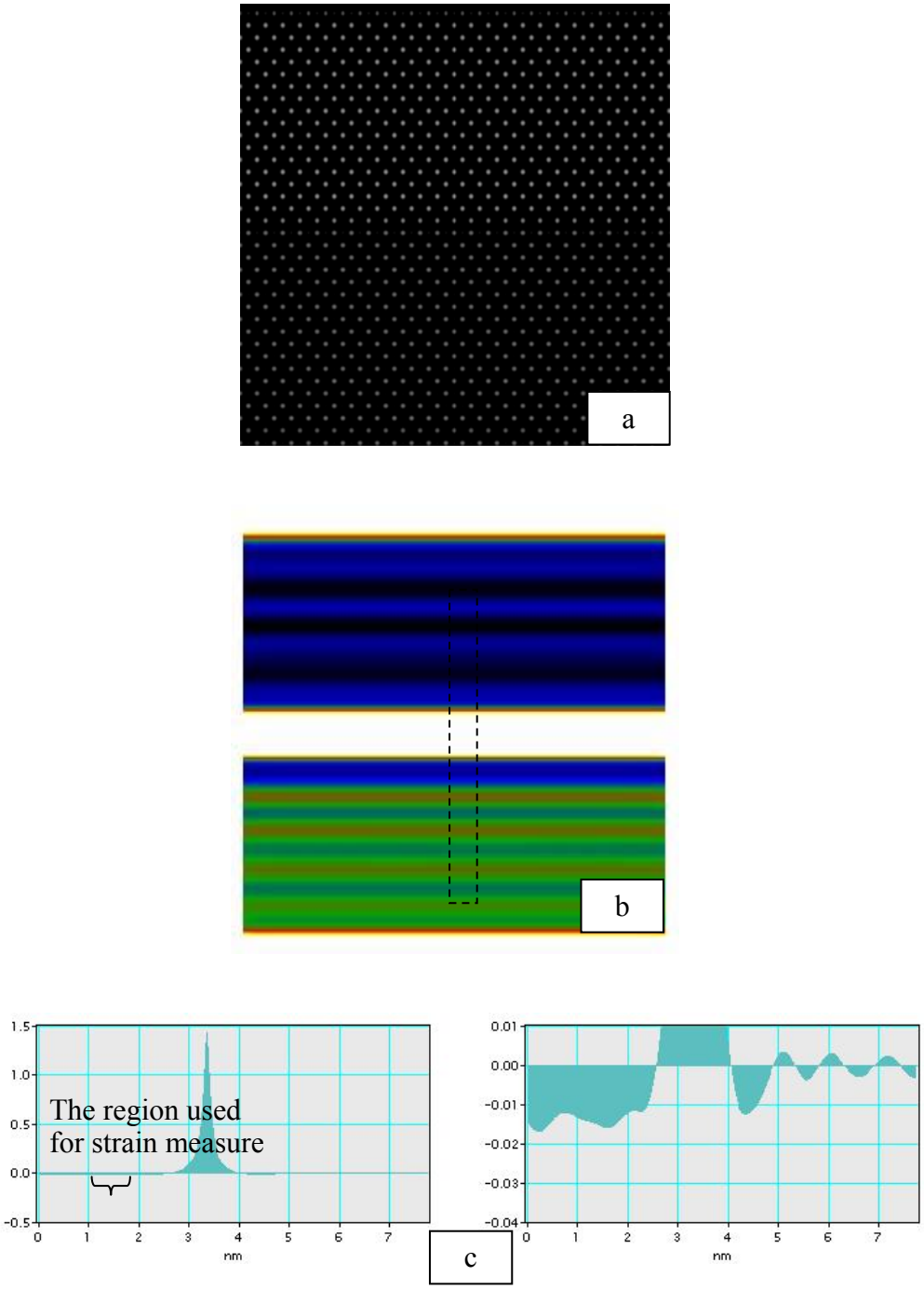

Figure 2.14: (a) HRTEM image of sSi on Cl substrate for *thickness* = 40nm, (b) relative strain map of (a), and line-scan plot of the dotted area in (b).

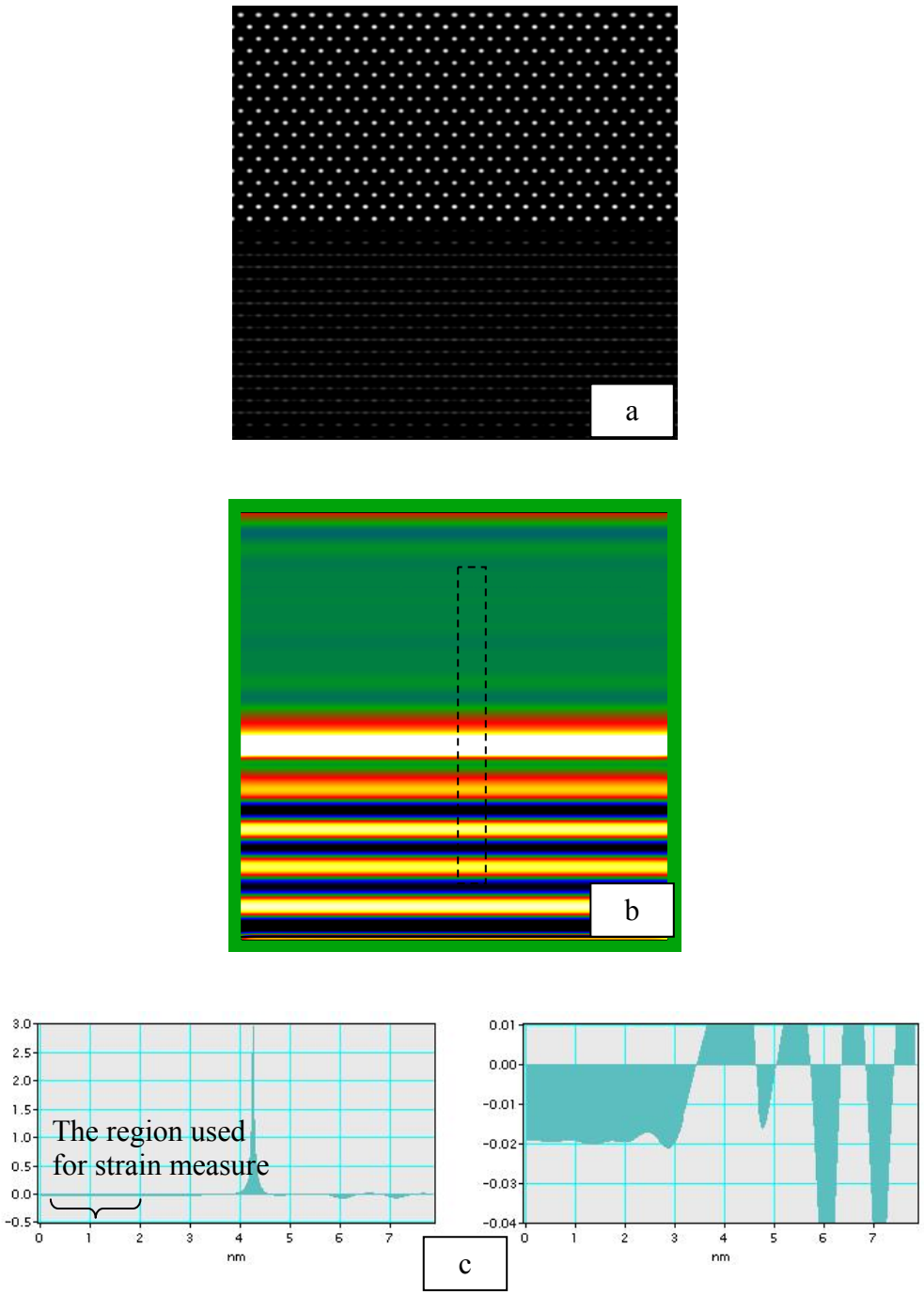

Figure 2.15: (a) HRTEM image of sSi on Cl substrate for *thickness* = 50nm, (b) relative strain map of (a), and line-scan plot of the dotted area in (b).

Relaxed area, $Si_{0.82}Ge_{0.18}$ Δf (nm)	**Mismatch (Relative strain, $e_{n\perp}$)**		
	Preset (%)	**Measured**	
		Average (%)	**Standard deviation (%)**
10	-1.26	-1.2304	0.0176
20	-1.26	-1.2411	0.01935
30	-1.26	-1.3804	0.5101
40	-1.26	-1.4470	0.1470
50	-1.26	-1.9581	0.03579

Table 2.2: Preset and measured mismatch data for sSi on Cl substrate for different sample thickness values.

2.1.3 Effect of C_s-Corrected Microscope on Measurement of Strain

The purpose of this section is to understand the effect of C_s corrected microscope to characterize strain using GPA technique from {111} Bragg beam.

HRTEM image of sSi layer on relaxed $Si_{82}Ge_{18}$ with $e_{n\perp}$ = -1.26 %, were simulated with the following conditions for a slightly negative spherical aberration coefficient:

Electron beam energy: 300KeV (λ = 0.00196 nm)

Spherical aberration coefficient of the objective lens, C_s: -0.005 mm

Chromatic aberration coefficient, C_c: 1.1 mm

Convergence half-angle: 1.0 mrad

Defocus change: +0.2 nm

Thickness of sample: ~10nm

$Si_{82}Ge_{18}$ with $e_{n\perp}$ = -1.26 %

Using $\boldsymbol{k}$ = 3.18 nm^{-1} for {111} beams in Si, C_s = -0.005 mm, and λ = 0.00196 nm, the Δf meeting the condition that $\nabla_k \chi(\boldsymbol{k})$ is zero is found to be +0.2 nm from Equation (2.1). Figure 2.16 (a), Figure 2.16 (b) and Figure 2.16 (c) show HRTEM image, strain map and the line-scan plots respectively. The measured mismatch was 1.1786 % with standard deviation of 0. 1286 %. The observed difference is due to the significant oscillations and the effect of artifacts observed at and near the interface. At this point of time, it is not clear where the oscillations are coming from. It can be noted that the dumbbells expected for HRTEM image when viewing diamond structure in <110> direction are resolved for this particular imaging conditions.

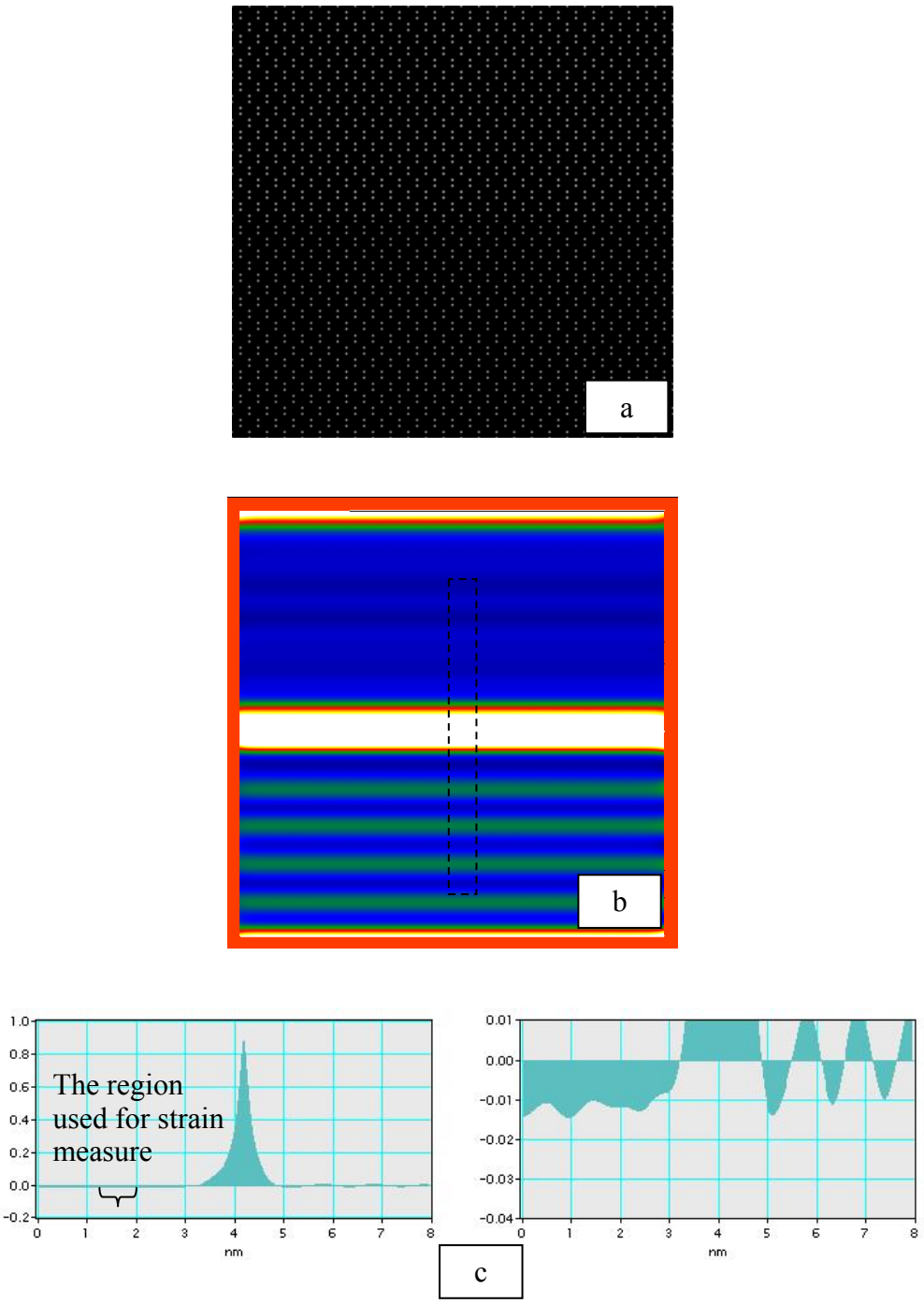

Figure 2.16: (a) HRTEM image of sSi on Cl substrate for C_s: -0.005mm, (b) relative strain map of (a), and line-scan plot of the dotted area in (b).

2.2 EFFECT OF SUDDEN CHANGE IN LATTICE CONSTANT (FAT SILICON SIMULATION)

As mentioned in the introduction, the effects of sudden lattice constant change on measurement of strain are analyzed in this section. Synthetic HRTEM images with known strain of 1.26% were created using Jems® software. As mentioned in the introduction, the $Si_{0.82}Ge_{0.18}$ alloy is represented by Si. The model for the simulated HRTEM images consists of a layer of strained Si on a relaxed, semi-infinite Si substrate as shown in Figure 2.17, where biaxial tensile strain exists only in the strained Si layer. The Ge concentration of the relaxed area controls the strain in the strained Si layer. The relative strain was calculated by the mismatch perpendicular to the hetero-interface using Equation (1.4). The atomic positions of the sSi (strained Si) layer in Figure 2.17 are displaced in the [001] direction according to Equation (1.3).

The HRTEM image simulated using the following imaging conditions is shown in Figure 2.18.

Electron beam energy: 300KeV (λ = 0.00196 nm)

Spherical aberration coefficient of the objective lens, C_s: 1.2 mm

Chromatic aberration coefficient, C_c: 1.1 mm

Convergence half-angle: 1.0 mrad

Defocus change: -47 nm

Thickness of sample: ~10 nm

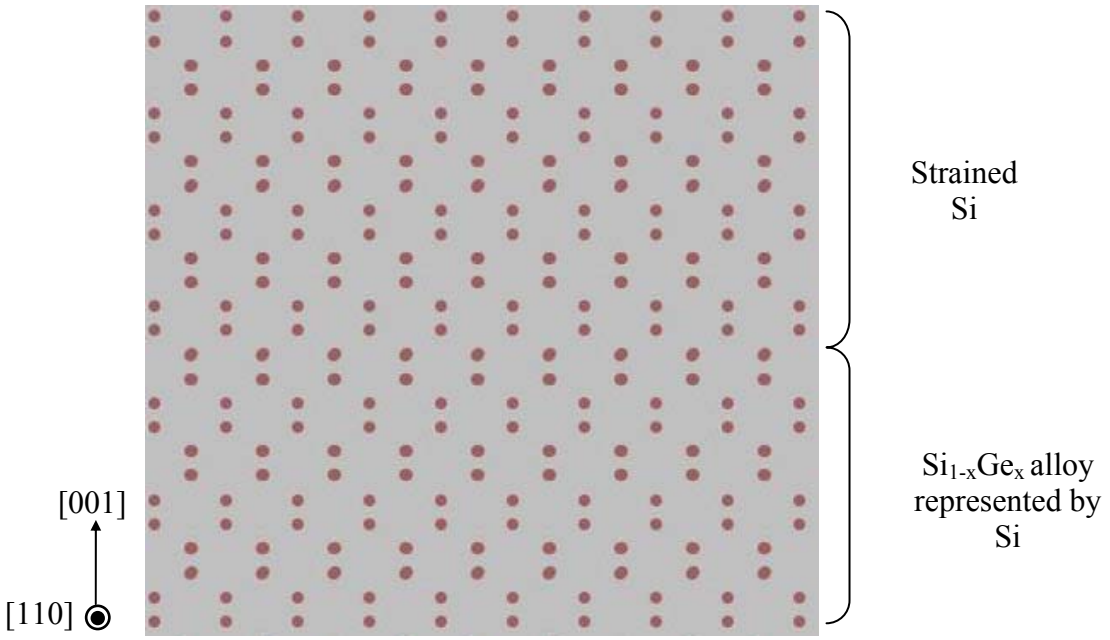

Figure 2.17: Atomic arrangement of sSi layer on relaxed $Si_{0.82}Ge_{0.18}$ alloy by Jems.

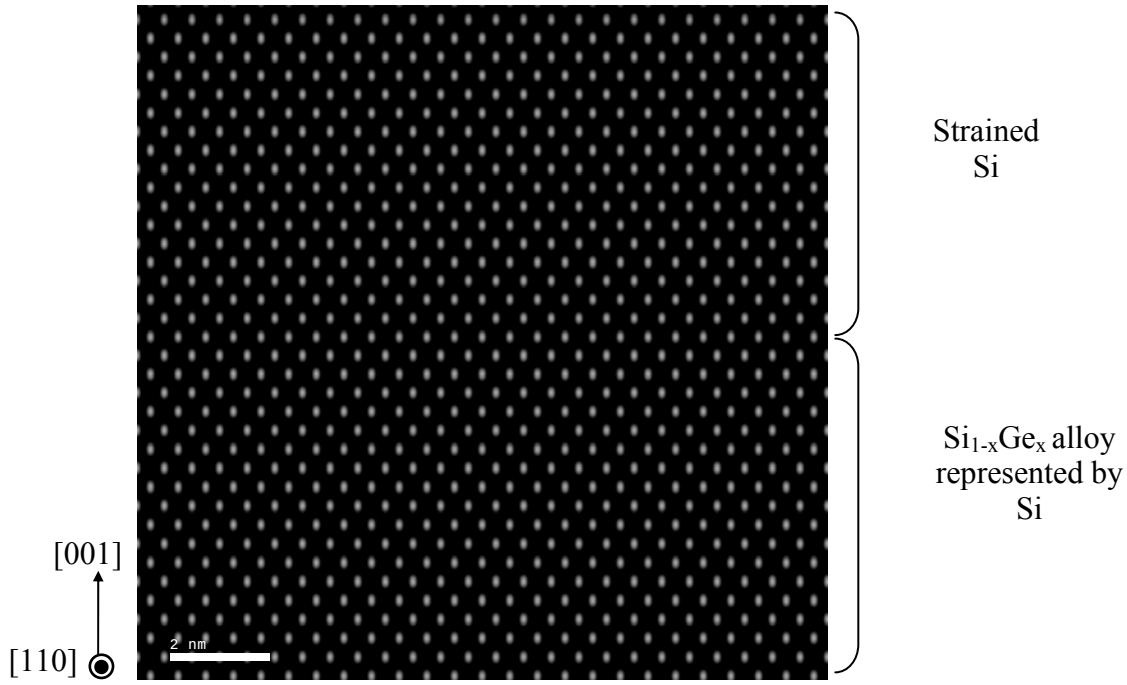

Figure 2.18: Simulated HRTEM image of sSi layer on relaxed $Si_{0.82}Ge_{0.18}$ by Jems.

2.2.1. Effect of Defocus on Apparent Strains Measured using {111} Beams

The purposes of this section are to examine the variation of measured strains with respect to changes in defocus and to determine the optimum defocus for accurate strain determination using the GPA technique from {111} Bragg beam from Si specimens.

Using $\boldsymbol{k}$ = 3.18 nm^{-1} for {111} beams in Si, C_s = 1.2 mm, and λ = 0.00196 nm, the Δf meeting the condition that $\nabla_k \chi(\boldsymbol{k})$ is zero is found to be -47 nm from Equation (2.1).

HRTEM images of a sSi layer on relaxed $Si_{82}Ge_{18}$ with $e_{n\perp}$ = -1.26 %, were simulated for various defocus values, keeping all other imaging conditions (C_s, C_c, λ, convergence half angle and sample thickness) constant. Figure 2.19 (a) through Figure 2.25 (a) show HRTEM images for Δf = -38 nm, Δf = -41nm, Δf = -44nm, Δf = -47nm, Δf = -50nm, Δf = -53nm and Δf = -56 nm, respectively. Each of these simulated images was processed using GPA and reconstructed as a strain map following the sequences developed by Chung. Figure 2.19 (b) through Figure 2.25 (b) show the reconstructed strain images for the same defocus values. Line-scan plots are displayed for each strain map in Figure 2.19 (c) through Figure 2.25 (c).

As expected, the effects of terms neglected in the derivation of the $\nabla_k \chi(\boldsymbol{k}) = 0$ criterion can be observed when analyzing the simulated HRTEM images and strain maps. Figure 2.19 (c) through Figure 2.25 (c) show artifacts resulting from various defocus values near the interface where strain changes from 0 % to -1.26 %.

Table 2.3 shows the mismatch values measured from the line scan plots for each HRTEM image. The average strain values and their standard deviation were measured in the center region of each strained layer in each line plot as shown in Figure2.19 (c) in order to exclude the effect of artifacts near interface. These results indicated that the measured mismatch values were in very good agreement with the preset values for cases

when Δf is less than the optimum defocus. The measured mismatch values increased from -1.2661 % to -1.2611 % for Δf varying from -38 nm to -47 nm (optimum defocus). For Δf varying from -47 nm to -56 nm, the measured mismatch increased by ~ 0.015% and also significant oscillations were noticed near the interface. As observed with the sSi on Cl substrate, at the optimum defocus, a change in trend is noticed in the measured strain values as shown in Figure 2.26. The strain mismatch value measured at the optimum defocus was -1.26% ± 0.014%.

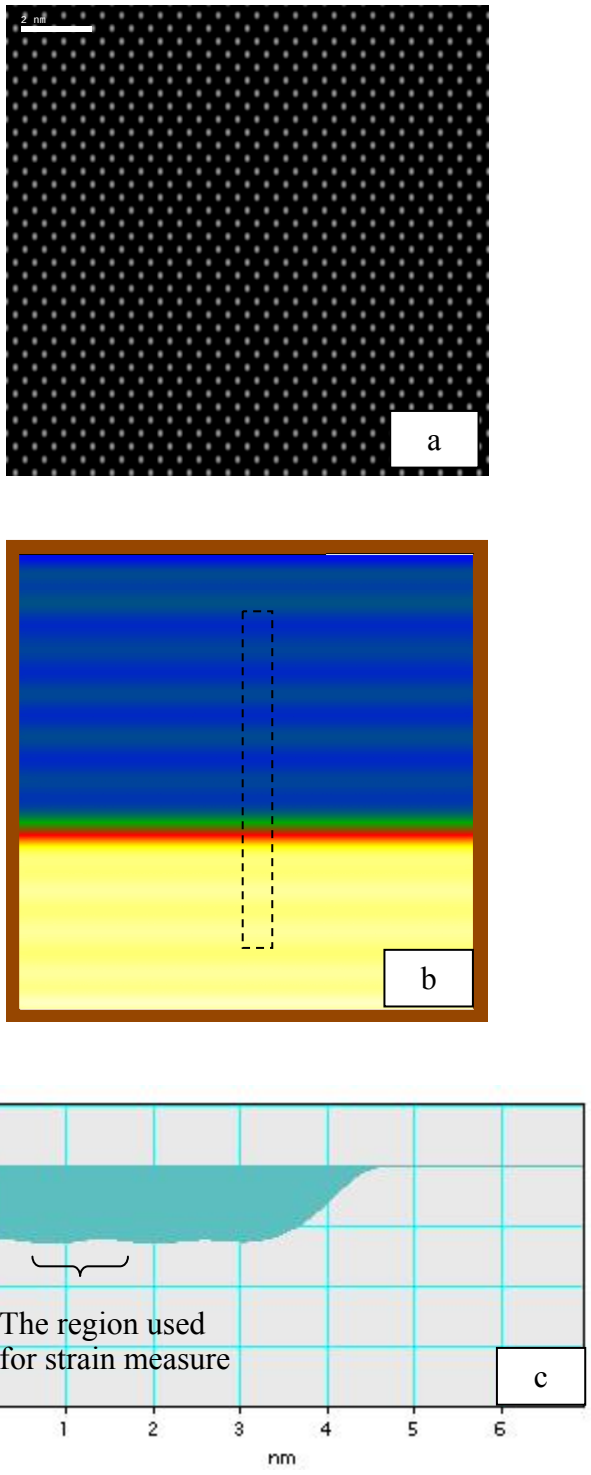

Figure 2.19: (a) HRTEM image of sSi on fat Si substrate for Δf = -38nm, (b) relative strain map of (a), and line-scan plot of the dotted area in (b).

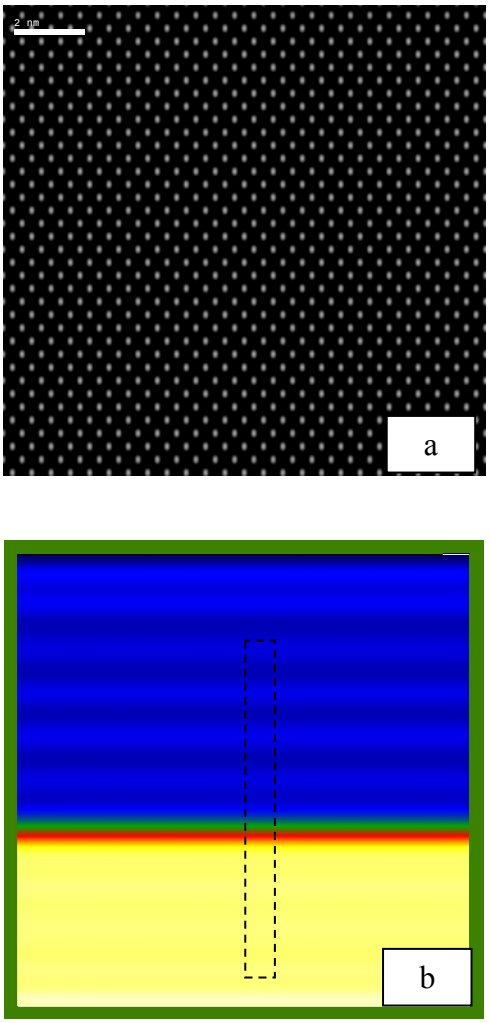

Figure 2.20: (a) HRTEM image of sSi on fat Si substrate for Δf = -41nm, (b) relative strain map of (a), and line-scan plot of the dotted area in (b).

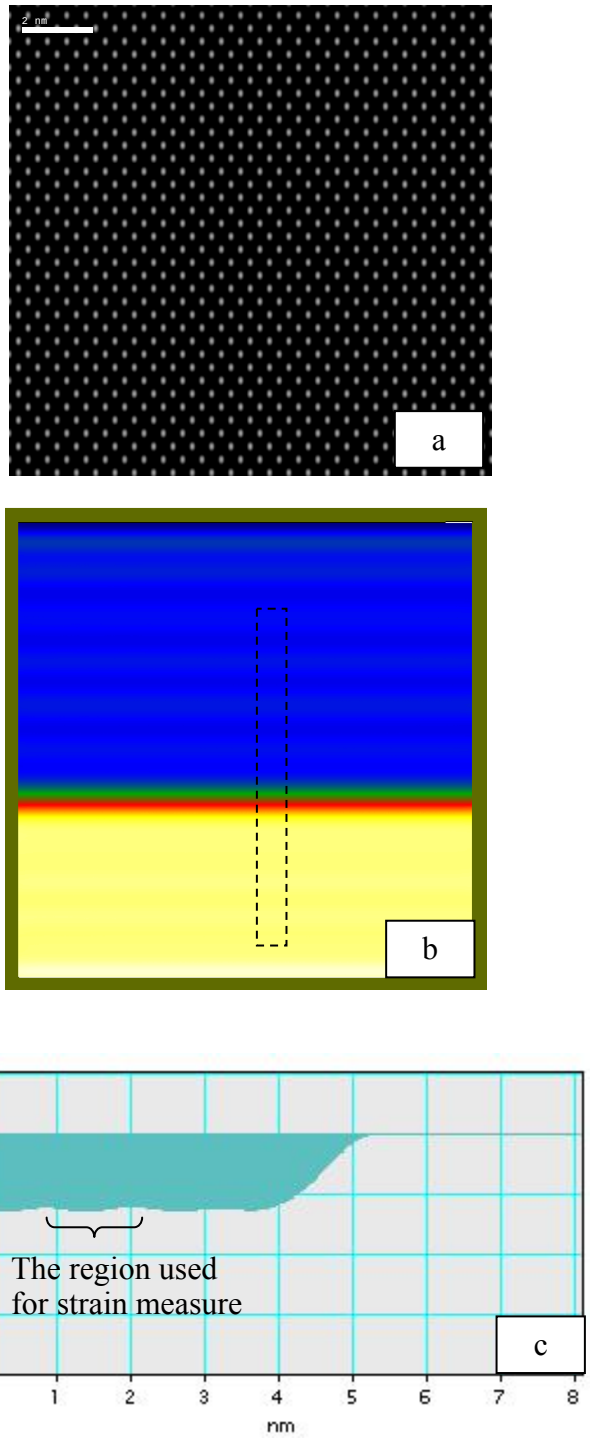

Figure 2.21: (a) HRTEM image of sSi on fat Si substrate for Δf = -44nm, (b) relative strain map of (a), and line-scan plot of the dotted area in (b).

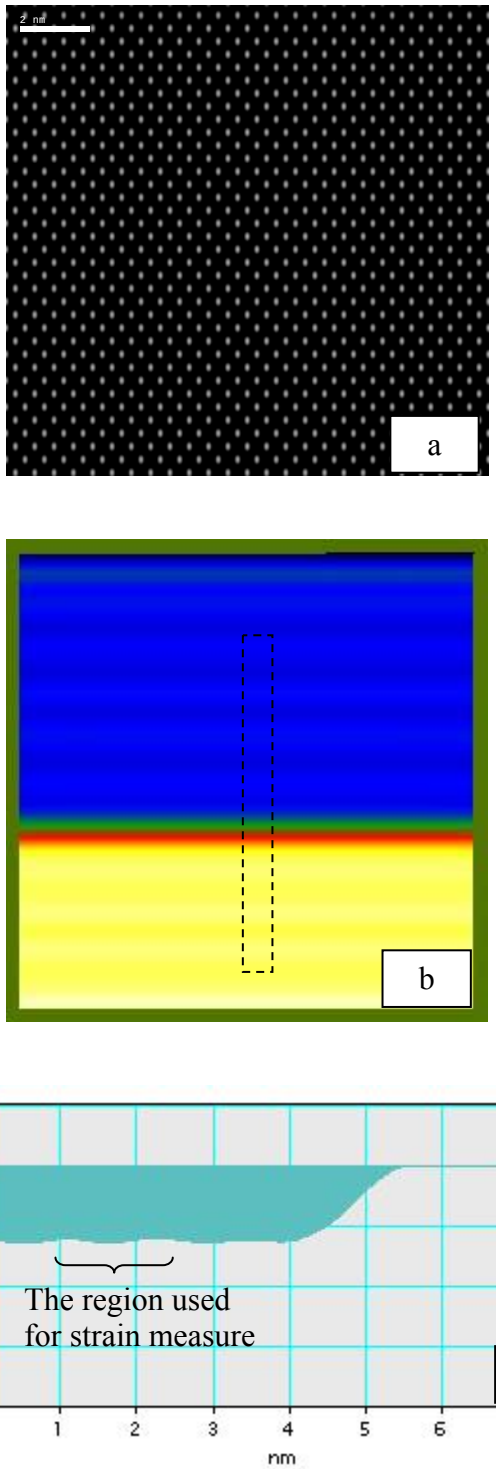

Figure 2.22: (a) HRTEM image of sSi on fat Si substrate for Δf = -47nm, (b) relative strain map of (a), and line-scan plot of the dotted area in (b).

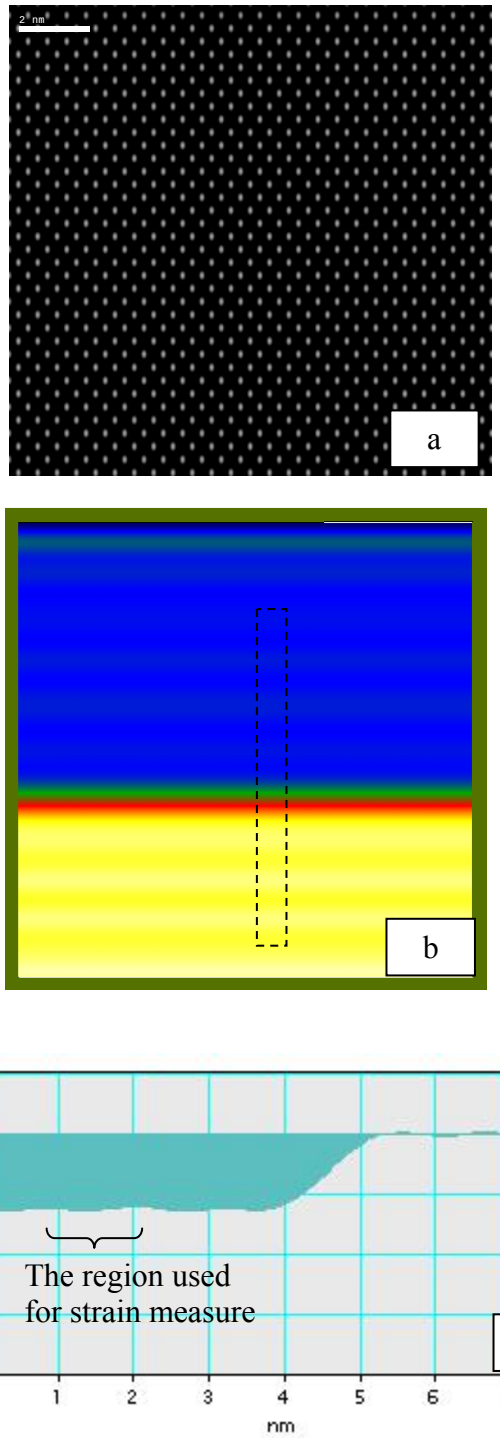

Figure 2.23: (a) HRTEM image of sSi on fat Si substrate for Δf = -50nm, (b) relative strain map of (a), and line-scan plot of the dotted area in (b).

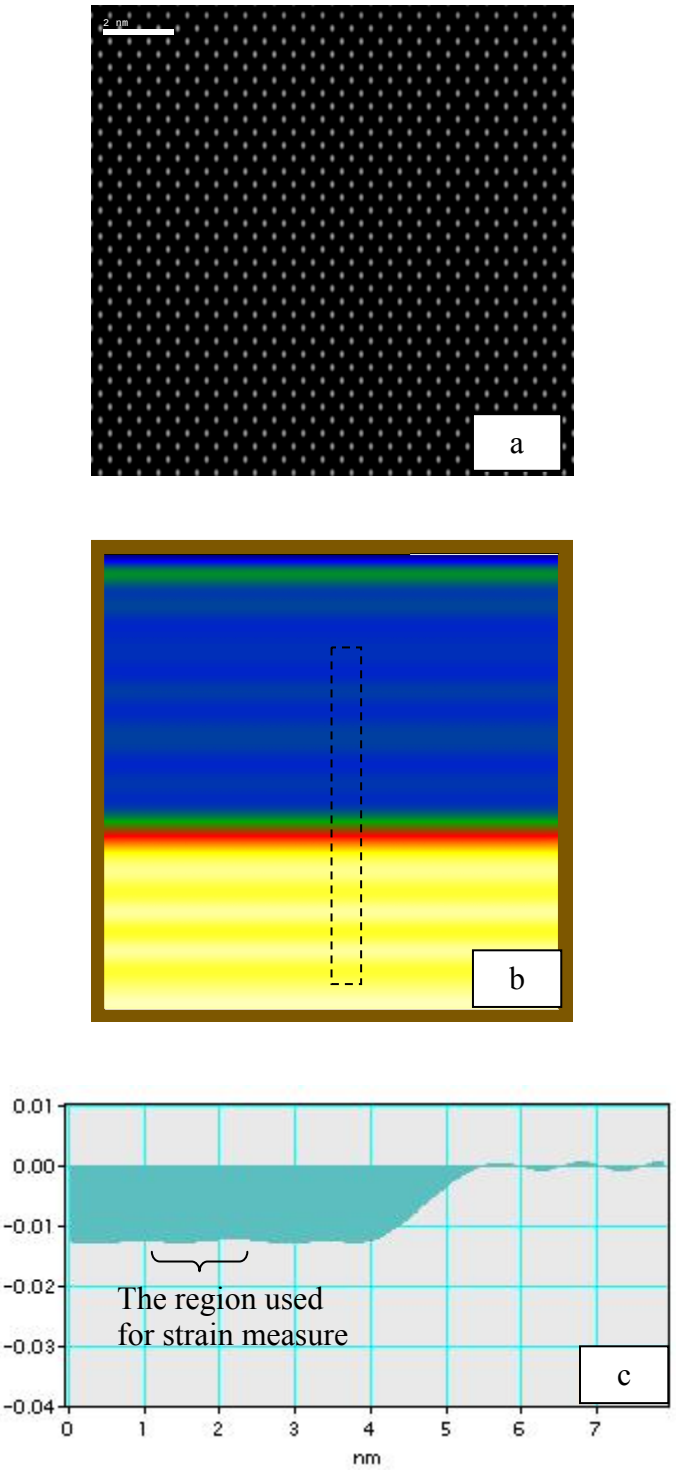

Figure 2.24: (a) HRTEM image of sSi on fat Si substrate for Δf = -53nm, (b) relative strain map of (a), and line-scan plot of the dotted area in (b).

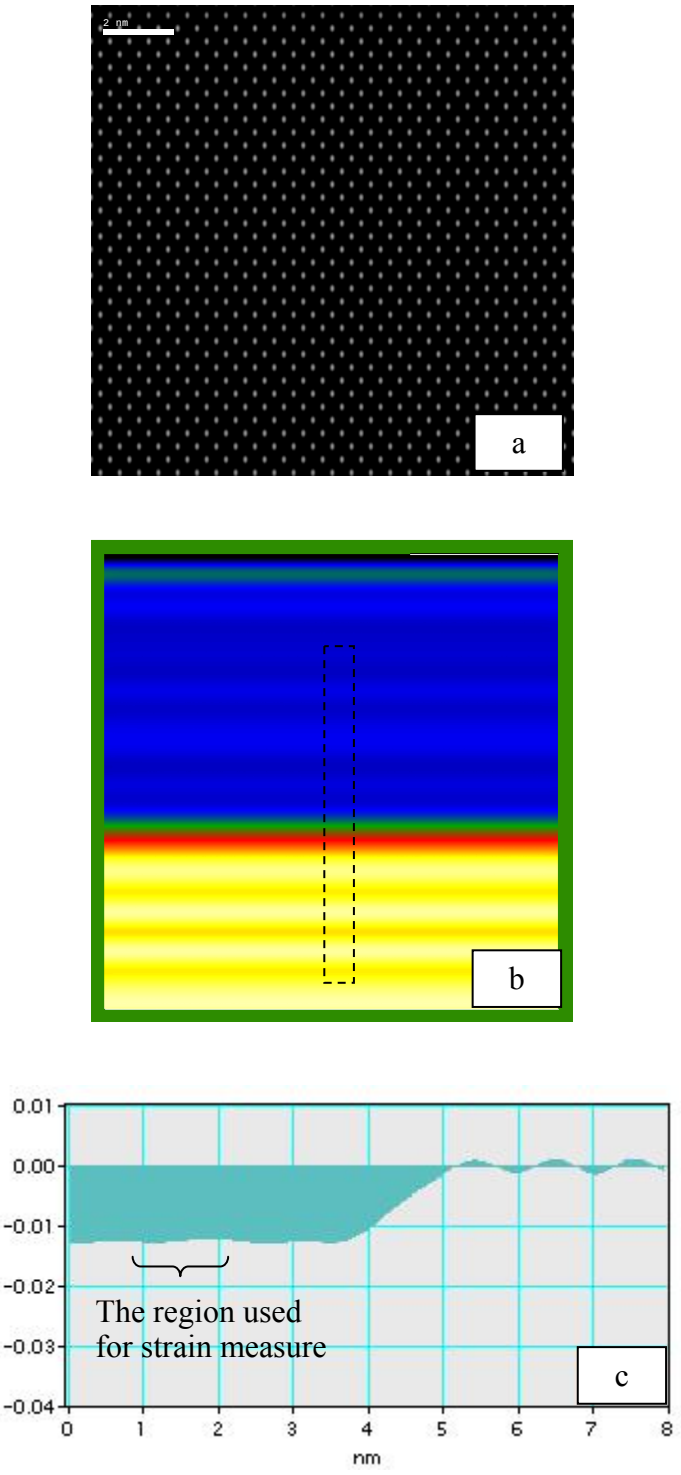

Figure 2.25: (a) HRTEM image of sSi on fat Si substrate for Δf = -56nm, (b) relative strain map of (a), and line-scan plot of the dotted area in (b).

Relaxed area, $Si_{0.82}Ge_{0.18}$ Δf (nm)	**Mismatch (Relative strain, $e_{n\perp}$)**		
	Preset (%)	**Measured**	
		Average (%)	**Standard deviation (%)**
-38	-1.26	-1.2661	0.0211763
-41	-1.26	-1.2633	0.0199273
-44	-1.26	-1.2613	0.0215187
-47	-1.26	-1.2611	0.0142575
-50	-1.26	-1.2723	0.0113699
-53	-1.26	-1.2725	0.0116462
-56	-1.26	-1.2757	0.006390

Table 2.3: Preset and measured mismatch data for sSi on fat Si substrate for different Δf values.

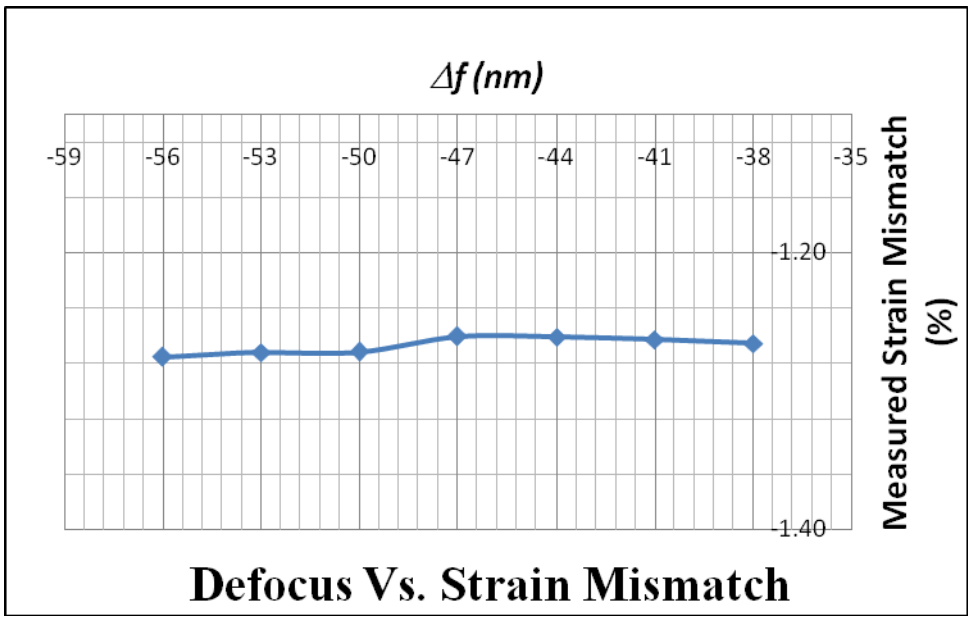

Figure 2.26: Preset and measured mismatch data for sSi on fat Si substrate for different Δf values.

2.2.2 Effect of C_s-Corrected Microscope on Measurement of Strain

The purpose of this section is to understand the effect of *Cs* corrected microscope to characterize strain using GPA technique from {111} Bragg beam when there is a change in lattice constant while the atomic number remains the same across the interface.

HRTEM image of sSi layer on relaxed $Si_{82}Ge_{18}$ with $e_{n\perp}$ = -1.26 %, were simulated with the following conditions for a slightly negative spherical aberration coefficient:

Electron beam energy: 300KeV (λ = 0.00196 nm)

Spherical aberration coefficient of the objective lens, *Cs*: -0.005 mm

Chromatic aberration coefficient, C_c: 1.1 mm

Convergence half-angle: 1.0 mrad

Defocus change: +0.2 nm

Thickness of sample: ~10nm

Using $\boldsymbol{k}$ = 3.18 nm^{-1} for {111} beams in Si, C_s = -0.005 mm, and λ = 0.00196 nm, the Δf meeting the condition that $\nabla_k \chi(\boldsymbol{k})$ is zero is found to be +0.2 nm from Equation (2.1). Figure 2.27 (a), Figure 2.27 (b) and Figure 2.27 (c) show HRTEM image, strain map and the line-scan plots respectively. The measured mismatch was 1.3359 % with standard deviation of 0. 03489 %. The observed difference is due to the significant oscillations and the effect of artifacts observed at and near the interface. The observed oscillations are far less for the fat silicon case compared to the sSi on Cl substrate case. As observed in HRTEM image from section 2.1.3, the dumbbells expected for HRTEM image when viewing diamond structure in <110> direction are resolved for this particular imaging conditions.

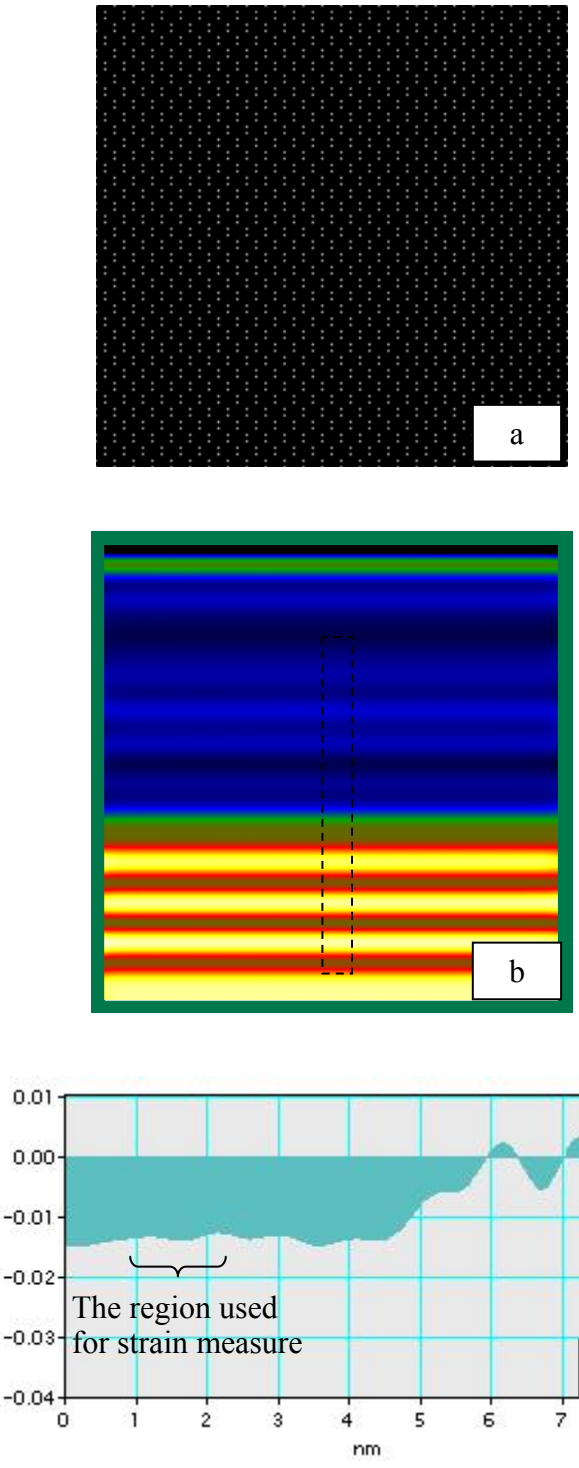

Figure 2.27: (a) HRTEM image of sSi on fat Si substrate for C_s: -0.005mm, (b) relative strain map of (a), and (c) line-scan plot of the dotted area in (b).

CHAPTER 3: CONCLUSION

From the simulation results presented in the previous chapter, the following conclusions can be made about the imaging conditions for characterization of local strain using GPA across a heteroepitaxial interface.

3.1 EFFECT OF DEFOCUS ON MEASUREMENT OF STRAIN

- As expected, the effects of higher-order terms neglected in the derivation of the $\nabla_k \chi(\mathbf{k}) = 0$ near an actual strain gradient were observed when the defocus value changed from -37 nm to -56 nm. This is seen from the fact that the oscillation amplitudes are sensitive functions of defocus. And, the oscillations amplitudes were smaller when there was only a sudden change in lattice constant.
- The measured mismatch values were in very good agreement (-1.23% ± 0.018% for strained silicon on chlorine substrate and -1.26% ± 0.014% for fat silicon) at optimum defocus.
- At the optimum defocus, a change in trend was noticed in the measured strain values.
- A sudden change in atomic number appeared to have caused significant ripples not only at the interface but also from the substrate. Strong oscillations from compression to tension were noticed at the interface.
- Even though a sudden change in lattice constant caused artifacts near the interface, the oscillations were of much lower amplitude when compared to the case of a sudden change in atomic number. The variation in

measured mismatch values was significantly lower, when the defocus changed from -38 nm through -56 nm.

3.2 Effect of Thickness on Measurement of Strain

- As expected, with the increase in sample thickness, significant oscillations were observed near the interface.
- A structure factor contrast was noticed with the increase in specimen thickness. The contrast in the HRTEM image was reversed as the thickness increased from 10 nm to 50 nm.
- The measured mismatch values were in close agreement with the preset values for sample of thickness 10 nm and 20 nm. Significant variation was observed from preset value for cases with sample thickness varying from 30 nm through 50 nm.

3.3 Effect of C_S-Corrected Microscope on Measurement of Strain

- The measured mismatch was -1.18% ± 0.129% for the strained silicon on chlorine substrate and about -1.34% ± 0.014% for the fat silicon case.
- Even though the system presents its ideal case where the objective lens transfer function is smooth and well behaved, the observed difference in measured values could possibly be due to significant oscillations and the effect of artifacts observed near the interface. The observed oscillations are far less when there is no local change in atomic number. At this point, there is no clear understanding about the source of the oscillations.

- The dumbbells expected for HRTEM image when viewing diamond structure in <110> direction were resolved for this particular imaging conditions.
- The simulated images show strong horizontal oscillations and weaker vertical oscillations as a result of image shrinkage in MS Word which is not observed at 100% size of the image.

3.4 SENSITIVITY OF STRAIN MEASUREMENT

- The strain mismatch and the standard deviations mentioned in the earlier chapter was measured in specific areas from the strained silicon away from the interface, where the oscillations observed in the line scan plots were less and appeared flat to the eyes.
- According to Hytch, the standard deviation of the fluctuations in a uniform part of the lattice gives the precision, and the length scale of these fluctuations gives the spatial resolution.
- According to Hytch and Chung, the spatial resolution calculated from the Gaussian mask of size 6σ applied in the Fourier space during image processing is 2.1 nm. The spatial resolution calculated from Figure 2.22 (C) that represents the optimum imaging conditions for pure strain measurements is 1.69 ± 0.025 nm.

Bibliography

[1] R. D. Isaac, IBM J. Res. Develop. 44, 369 (2000).

[2] R.R. Schaller, IEEE Spectrum, 52 (1997).

[3] J. Welser, J. L. Hoyt, S. Takagi, J. F. Gibbons, International Electron Devices Meeting 1994 Technical Digest., 373 (1994).

[4] D. K. Nayak, J. C. S. Woo, J. S. Park, K. L. Wang, and K. P. MacWilliams, Appl. Phys. Lett. 62, 2853 (1993).

[5] I. De Wolf, H. Norström, H. E. Maes, J. Appl. Phys. 74, 4490 (1993).

[6] Y. Ando, J. R. Patel, N. Kato, J. Appl. Phys. 44, 4405 (1973).

[7] A. Dimoulas, P. Tzanetakis, A. Georgakilas, O. J. Glembocki, and A. Christou, J. Appl. Phys. 67, 4389 (1990).

[8] V. Senez, A. Armigliato, I. De Wolf, G. Carnevale, R. Balboni, S. Frabboni, and A. Benedetti, J. Appl. Phys. 94, 5574 (2003).

[9] A. Toda, N. Ikarashi, H. Ono, and K. Okonogi, Appl. Phys. Lett. 80, 2278 (2002).

[10] S. L. Toh, K. P. Loh, C. B. Boothroyd, K. Li, C. H. Ang, and L. Chan, J. Vac. Sci. Technol. 23, 940 (2005).

[11] A. Benedetti, A. G. Cullis, A. Armigliato, R. Balboni, S. Frabboni, G. F. Mastracchio, and G. Pavia, Appl. Surf. Sci. 188, 214 (2002).

[12] K. W. Ang, K. J. Chui, V. Bliznetsov, C. H. Tung, A. Du, N. Balasubramanian, G. Samudra, M. F. Li, and Y. C. Yeo, Appl. Phys. Lett. 86, 093102 (2005).

[13] M. J. Hÿtch, E. Snoeck, and R. Kilaas, Ultramicroscopy 74, 131 (1998).

[14] E. Snoeck, B. Warot, H. Ardhuin, A. Rocher, M. J. Casanove, R. Kilaas, and M. J. Hÿtch, Thin Solid Films 319, 157 (1998).

[15] M. J. Hÿtch, T. Plamann, Ultramicroscopy 87, 199 (2001).

[16] M. J. Hÿtch, J. L. Putaux, and J. M. Pénisson, Nature 423, 270 (2003).

[17] M. De Graef, Introduction to Conventional Transmission Electron Microscopy, Cambridge University Press, Cambridge (2003).

[18] Jayhoon Chung, Ph. D. Thesis, The University of Texas at Austin (2006).

[19] C. G. Van de Walle, and R. M. Martin, Phys. Rev. B 34, 5621 (1986).

[20] A. Rosenauer, Transmission Electron Microscopy of Semiconductor Nanostructures, Springer, Berlin (2003).

[21] http://cimewww.epfl.ch/people/stadelmann/jemsWebSite/jems.html.

[22] L. Reimer, Transmission Electron Microscopy: Physics of Image Formation and Microanalysis , Springer, Berlin (1997).

[23] Chung, and L. Rabenberg, Appl. Phys. Lett. 88, 013106 (2006).

[24] Chung, and L. Rabenberg, Ultramicroscopy 108, 1595 (2008).

Vita

Srivaramangai (Sri) Rajagopalan was born in Tamil Nadu, India, on October 21, 1979, the daughter of Raman Rajagopalan and Radha Rajagopalan. She received the Bachelor of Technology degree in Chemical Engineering from Anna University, India, in 2001, and the Master of Science in Chemical Engineering from University of Florida, USA, in 2003. She worked for Intel Corporation, USA, from February 2004 to August 2004. In January 2006, she joined the Texas Materials Institute of the University of Texas at Austin and pursued her MSE in Material Science and Engineering. During the MSE program, she worked for Samsung Austin Semiconductors, USA.

Permanent address: 1403 River Birch Way, Pflugerville, TX-78660.

Email address: linked.sri@gmail.com.

This thesis was typed by Srivaramangai Rajagopalan.